

Aneuploidy can be an evolutionary detour on the path to adaptation

Ilia Kohanovski^{a,b,*}, Martin Pontz^{a,*}, Orna Dahan^c, Yitzhak Pilpel^c, Avihu H.
Yona^d, and Yoav Ram^{a,1}

^aSchool of Zoology, Faculty of Life Sciences, Tel Aviv University, Tel Aviv, Israel

^bSchool of Computer Science, Reichman University, Herzliya, Israel

^cDepartment of Molecular Genetics, Weizmann Institute of Science, Rehovot 76100, Israel

^dInstitute of Biochemistry, Food Science and Nutrition, Robert H. Smith Faculty of Agriculture, Food and Environment, The Hebrew University of Jerusalem, Israel

*These authors contributed equally to this work

¹Corresponding author: yoav@yoavram.com

October 30, 2022

Classifications. Biological Sciences: Evolution, Genetics, Microbiology, Population Biology.

Keywords: whole-chromosome duplication, evolutionary model, adaptive evolution

Abstract

16 Aneuploidy is common in eukaryotes, often leading to decreased growth and fitness. However,
evidence from yeast and fungi, as well as human tumour cells, suggests that specific aneuploidies
18 can be beneficial under stressful conditions and facilitate adaptation. In a prominent example, an
evolutionary experiment with yeast, populations evolving under heat stress had become aneuploid
20 (chromosome III), only to later revert back to euploid after genetic mutations have accumulated. It
has therefore been suggested that aneuploidy serves as a "stepping stone" on the path to adaptation.

22 Here, we test this hypothesis. First, we apply DNA sequencing to show that mutant alleles
common in aneuploid cells are uncommon in the evolved euploid population. Second, we develop
24 an evolutionary model with both aneuploidy and mutation, and fit it to the results of the experiment
using a Bayesian inference framework. We then predict the genotype frequency dynamics during
26 the experiment, demonstrating that the majority of the evolved euploid population likely did not
descend from aneuploid cells, but rather directly from the euploid wild-type population. Our
28 model further predicts that if the experiment was repeated with smaller populations, then a larger
fraction of the evolved population would descend from aneuploid cells.

30 Together, our results suggest that aneuploidy can be an inevitable evolutionary "detour" rather
than a "stepping stone": it can delay, rather than facilitate, the adaptation of the population, and
32 cells that become aneuploid may leave less descendants compared to cells that remain diploid.

Introduction

34 Aneuploidy is an imbalance in the number of chromosomes in the cell: an incorrect karyotype.
Evidence suggests aneuploidy is very common in eukaryotes, e.g. animals^{39,30,2}, and fungi^{33,62,37,51}.
36 Aneuploidy has been implicated in cancer formation, progression, and drug resistance^{4,41,39,19}. It
is also common in protozoan pathogens of the *Leishmania* genus, a major global health concern²⁸,
38 and contributes to the emergence of drug resistance⁴² and virulence²⁹ in fungal pathogens, which
are under-studied³⁸, despite infecting a billion people per year, causing significant morbidity in >150
40 million and death in >1.5 million people per year^{42,38}.

Experiments with human and mouse embryos found that most aneuploidies are lethal. It is also
42 associated with developmental defects and lethality in other multicellular organisms⁴⁵. For example,
aneuploid mouse embryonic cells grow slower than euploid cells⁵⁶. Similarly, in unicellular eukaryotes
44 growing in benign conditions, aneuploidy usually leads to slower growth and decreased overall
fitness^{31,54,33,45,22,57}, in part due to proteotoxic stress caused by increased expression in aneuploid
46 cells^{33,40,61} and hypo-osmotic-like stress⁵⁵.

However, aneuploidy can be beneficial under stressful conditions due to the wide range of phenotypes
48 it can produce, some of which are advantageous^{33,57}. Indeed, in a survey of 1,011 yeast strain,
aneuploidy has been detected in about 19%³⁴. Thus, aneuploidy can lead to rapid adaptation in
50 unicellular eukaryotes^{14,53,18,36}, as well as to rapid growth of somatic tumour cells^{41,47}. For example,
aneuploidy in *Saccharomyces cerevisiae* facilitates adaptation to a variety of stressful conditions
52 like heat and pH⁵⁹, copper^{7,14}, salt¹⁰, and nutrient limitation^{11,16,1}, with similar results in *Candida albicans*⁵⁷. Importantly, aneuploidy can also lead to drug resistance in pathogenic fungi such as
54 *C. albicans*^{44,43,13} and *Cryptococcus neoformans*⁴⁸, which cause candidiasis and meningoencephalitis,
respectively.

56 Yona et al.⁵⁹ demonstrated experimentally the importance of aneuploidy in adaptive evolution. They
evolved populations of *S. cerevisiae* under strong heat stress. The populations adapted to the heat stress
58 within 450 generations, and this adaptation was determined to be due a duplication of chromosome III.
Later on, after more than 1,500 generations, the populations reverted back to an euploid state, while
60 remaining adapted to the heat stress. Aneuploidy was therefore suggested to be a *transient adaptive solution*, because it can rapidly appear and fixate in the population under stressful conditions, and can
62 then be rapidly lost when the cost of aneuploidy outweighs its benefit—after the stress is removed,
or after "refined" beneficial mutations appear and fixate⁵⁹. Furthermore, it has been suggested that
64 aneuploidy is an evolutionary "stepping stone" that facilitates future adaptation by genetic mutations,

which require more time to evolve^{59,58}.

66 Here, we test the hypothesis that aneuploidy is a *an evolutionary stepping stone* that facilitates adaptive
evolution by genetic mutations. First, we sequenced the genomes of evolved populations reported in⁵⁹
68 and analyzed their mutant allele frequencies to assess if the evolved euploid cells are descended from
aneuploid cells. Second, we develop an evolutionary genetic model and fit it to the experimental
70 results of Yona et al.⁵⁹ in order to predict the genotype frequency dynamics in the experimental
populations, thereby estimating the frequency of evolved euploid cells that descended from aneuploid
72 cells. Our results show that aneuploidy reached high frequencies in the experimental populations,
but nevertheless, the majority of cells in the evolved euploid population likely did not descend from
74 aneuploid cells, but rather directly from wild-type euploid cells. These results suggest that at the
lineage level, aneuploidy may be an evolutionary detour, rather than a stepping stone, on the path to
76 adaptation.

Results

78 In the heat-stress experiment of Yona et al.⁵⁹, four populations of *S. cerevisiae* evolved under 39 °C.
Aneuploidy fixed in all four experimental repetitions in the first 450 generations. Two of the repetitions,
80 marked *H2* and *H4*, carried no large-scale duplications other than a chromosome III trisomy. These
two repetitions continued to evolve under the same conditions, wherein aneuploidy was eliminated by
82 generation 1,700 and 2,350 in *H4* and *H2*, respectively.

Empirical frequencies of mutant alleles. For each of two evolved populations (*H2* and *H4*) we
84 sequenced the ancestral diploid population (generation 0), the aneuploid population (generation 450),
and the evolved euploid population (generation 1,700 or 2,350) to estimate the mutant allele frequencies
86 (Tables S1 and S2). Overall, between 100 and 173 mutant alleles were detected with at least a single
read in the six populations that were sampled. Disregarding 45 and 40 alleles that were present in
88 the ancestral populations at a frequency >10%, the aneuploid and euploid populations carried a large
number of mutant alleles: 82 and 95, respectively, in repetition *H2*, and 60 and 66 in repetition
90 *H4*.

Surprisingly, out of all these mutant alleles, none was present at a frequency >20% in both the
92 aneuploid and the evolved euploid populations. More importantly, a high mutant allele frequency
in the aneuploid population was associated with a low frequency in the evolved euploid population,
94 and vice-versa (Spearman's correlation coefficient $\rho = -0.64$ and -0.66 in the two experimental

repetitions; Figure 1), suggesting that mutant alleles frequent in the aneuploid populations decreased
96 in frequency when aneuploidy was lost. These results suggest evolved euploid cells are unlikely to
descend from aneuploid cells.

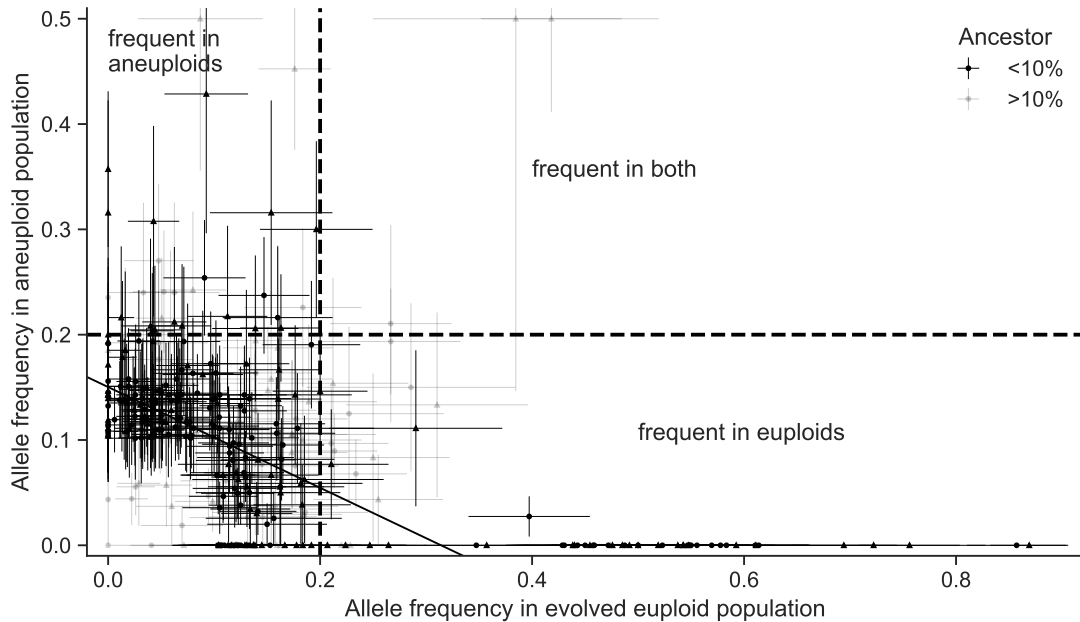


Figure 1: Frequencies of mutant alleles in the experimental populations are negatively correlated. Frequencies of mutant alleles when trisomy was widespread in the population (y-axis) and after it was eliminated (x-axis) in two experimental repetitions (circles for *H2* and triangles for *H4*) from Yona et al.⁵⁹. Mutant alleles with >20% in the aneuploid population were <20% in the euploid population, and vice versa (the upper-right quadrant is empty), suggesting that the majority of evolved euploid cells did not descend from the most common aneuploid genotypes. Alleles with frequency below and above 10% in the ancestral populations are in black and gray, respectively. Solid black line is a linear orthogonal distance regression line (slope=−0.559, intercept=0.164; a regression through alleles that reach at least 20% in one of the populations has slope=−0.645 and intercept=0.297). Dashed vertical and horizontal lines show allele frequencies 20%. Error bars show standard error of the mean accounting for the number of reads. For the 18 mutant alleles with high frequency in the aneuploid populations (>20%), the highest frequencies in the euploid populations were 15.4%, 16%, 16.3% and 19.6% (the rest were below 15%). Similarly, for the 48 mutant alleles with high frequency in the evolved euploid populations, the highest frequencies in the aneuploid populations were 2.7%, 7.7%, and 11.1% (the rest were below 1%).

98 **Evolutionary genetic model.** To explore the dynamics during the evolutionary experiments, we
developed an evolutionary genetic model, fitted the model to empirical data, and used it to predict the
100 genotype frequency dynamics, or specifically, the fraction of the evolved euploid population descended

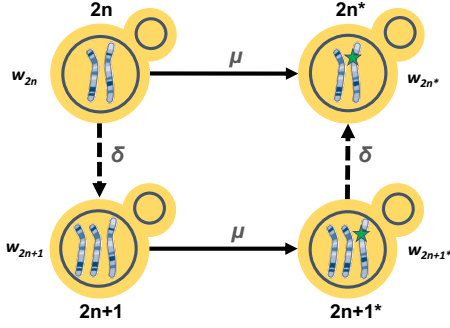


Figure 2: Model Illustration. There are four genotypes in our model: euploid wild-type, $2n$; euploid mutant, $2n^*$; aneuploid wild-type, $2n+1$; and aneuploid mutant, $2n+1^*$. Overall there are two possible trajectories from $2n$ to $2n^*$. Arrows denote transitions between genotypes, with transition rates μ for the beneficial mutation rate and δ for the aneuploidy rate.

from aneuploid cells.

102 The model includes the effects of natural selection, genetic drift, aneuploidy, and mutation, and follows
 103 a population of cells characterized by their genotype: euploid wild-type, $2n$, is the ancestral diploid
 104 genotype; euploid mutant, $2n^*$, has a diploid karyotype and a single beneficial mutation; aneuploid
 105 wild-type, $2n+1$, has an extra chromosome due to a chromosome duplication event; and aneuploid
 106 mutant, $2n+1^*$, has an extra chromosome and a beneficial mutation. Fitness values of the different
 107 genotypes are denoted by w_{2n} , w_{2n^*} , w_{2n+1} , and w_{2n+1^*} , and the rate of mutation and aneuploidy are
 108 denoted by μ and δ . See Figure 2 for an illustration of the model.

We fitted this model to the experimental results⁵⁹ – time for fixation ($>95\%$) and for loss ($<5\%$) of
 110 aneuploidy – using approximate Bayesian computation with sequential Monte Carlo (ABC-SMC)⁴⁹,
 thereby inferring the model parameters: rates aneuploidy and mutation and the fitness of all genotypes.
 112 We then sampled posterior predictions for the genotype frequency dynamics using the estimated
 113 parameter values and compared different versions of the model to test additional hypotheses about the
 114 evolutionary process.

Estimated rates and fitness effects of aneuploidy and mutation. We inferred the posterior distribution of model parameters (Figure 3). We report parameter estimates using the MAP (maximum a posteriori) and providing the 50% HDI (highest density interval) in square brackets. See Supplementary Material for sensitivity analysis.

The estimated beneficial mutation rate is $\mu = 2.965 \cdot 10^{-6}$ [$2.718 \cdot 10^{-7} - 3.589 \cdot 10^{-6}$]. From the
 115 literature, the mutation rate per base pair is roughly $2 - 3 \cdot 10^{-10}$ (refs.^{63,27}), but it may be higher

under heat stress, as several stresses may cause hypermutation in yeast¹⁷. If we assume a 10-fold
122 increase in mutation rate, then the estimated beneficial mutation rate can be explained by a target size
of 1,000 base pairs. Yona et al.⁵⁹ found at least 10 genes on chromosome III with mutations that
124 led to increased heat tolerance. Assuming that other chromosomes also have a similar number of
heat-tolerance genes (i.e., chromosome III is one of the smaller chromosomes¹⁵), and that each gene
126 has a target size of ten base pairs, we easily get to a target size above 1,600.

The estimated aneuploidy rate, $\delta = 1.72 \cdot 10^{-3}$ [$1.47 \cdot 10^{-3} - 2.786 \cdot 10^{-3}$] is higher than in previous
128 studies: for chromosome III in diploid *S. cerevisiae*, Zhu et al.⁶³ estimated $6.7 \cdot 10^{-6}$ chromosome
gain events per generation, and Kumaran et al.²⁶ estimate $3.0 - 4.3 \cdot 10^{-5}$ chromosome loss events
130 per generation (95% confidence interval). However, this difference may be explained by an increased
aneuploidy rate during heat stress⁵.

132 The estimated fitness values are $w_{2n+1} = 1.022$ [1.021 – 1.023], $w_{2n+1*} = 1.025$ [1.024 – 1.026],
 $w_{2n*} = 1.028$ [1.026 – 1.029], all relative to the fitness of $2n$, which is set to $w_{2n} = 1$. Thus, we
134 can infer that the cost of chromosome III trisomy is $c = w_{2n*} - w_{2n+1*} = 0.003$ (or 0.3%) and the
benefit of trisomy is $w_{2n+1} - 1 - c = 0.019$ (1.9%), whereas the benefit of the beneficial mutation is
136 $w_{2n*} - 1 = 0.028$ (2.8%).

If we allow for transitions (mutation, chromosome loss and gain) to less-fit genotypes (e.g., $2n^*$ to
138 $2n+1^*$), then we infer similar but slightly different values, see Supplementary Material.

Model comparison and goodness-of-fit. Our model fits the data well: in simulations using the MAP
140 parameter estimates, $2n^*$ fixed in 61% of simulations by generation 1,700 and in 100% of simulations
by generation 2,350 (Figure 4B).

142 However, a model without aneuploidy (where the aneuploidy rate is fixed at zero, $\delta = 0$), fails to
explain the experimental observations (Figure 4). The estimated mutation rate without aneuploidy
144 is $\mu = 7.98 \cdot 10^{-9}$ [$7.906 \cdot 10^{-9} - 8.138 \cdot 10^{-9}$], much lower compared to a model with aneuploidy
and suggesting a target size of just 40. The fitness of the mutant is also much lower at $w_{2n*} =$
146 1.013 [1.012 – 1.013]. This is because, without aneuploidy, a high mutation rate or fitness effect will
lead to faster appearance and fixation of $2n^*$ than in the experimental observations.

148 We also checked a model in which aneuploidy occurs but is adaptively neutral compared to the wild-
type, that is, $w_{2n+1} = w_{2n}$ and $w_{2n+1*} = w_{2n*}$ but $\delta > 0$. This model fits the data better than the model
150 with no aneuploidy (in which $\delta = 0$), but worse than a model with positive selection for aneuploidy,
in which $w_{2n} < w_{2n+1} < w_{2n+1*} < w_{2n*}$ (Figure 4).

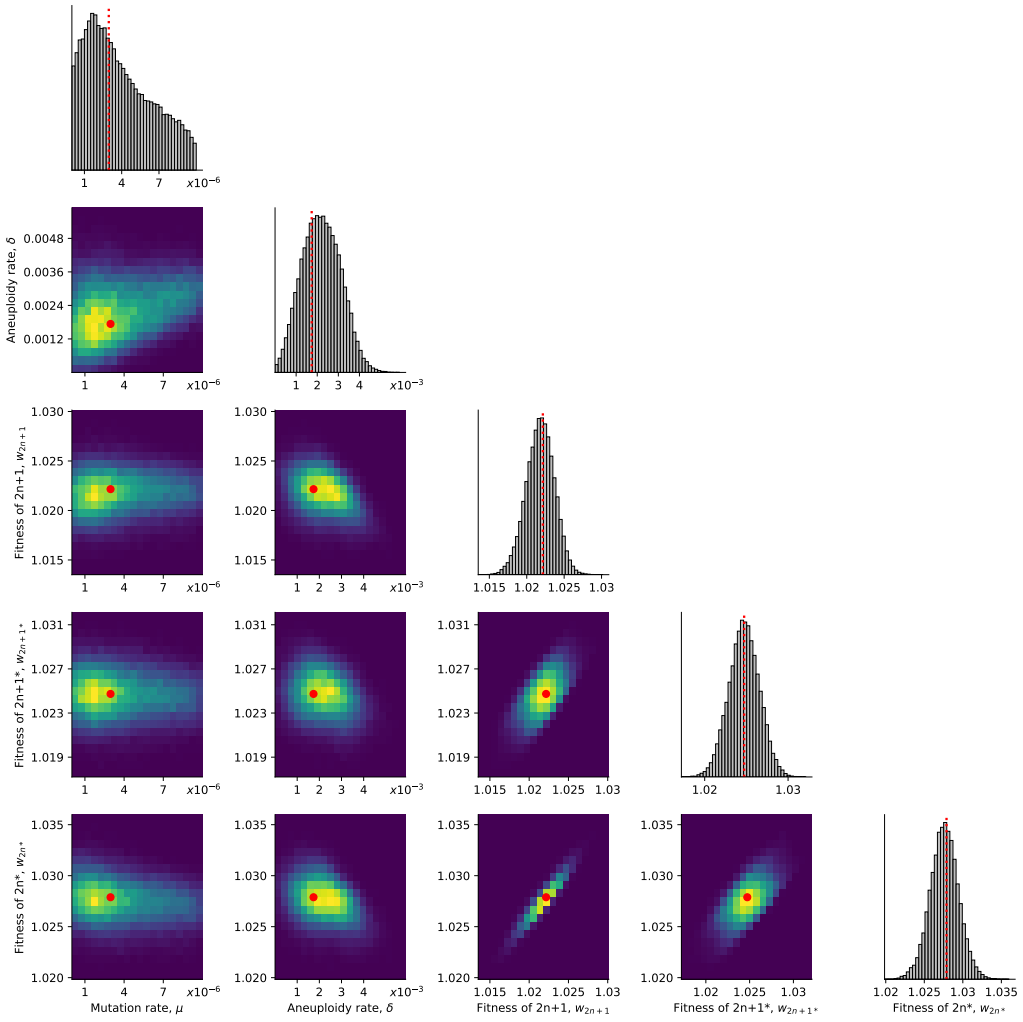


Figure 3: Posterior distribution of model parameters. On the diagonal, the marginal posterior distribution of each model parameter. Below the diagonal, the joint posterior distribution of pairs of model parameters (dark purple and bright yellow for low and high density, respectively). Red markers and orange lines for the joint MAP estimate (which may differ from the marginal MAP, as the marginal distribution integrates over all other parameters).

152 **Model predictions of genotype frequency dynamics.** We simulated 50 replicate genotype frequency dynamics using the MAP estimate parameters. Figure 5A shows the simulated frequencies of

154 the four genotypes ($2n$, $2n+1$, $2n+1^*$ and $2n^*$), as well as the frequencies of $2n^*$ cells that arose from either $2n+1$ cells via a sequences of mutation and chromosome loss events ($2n_A^*$), or directly from

156 $2n$ cells via a mutation event ($2n_M^*$). We find that $2n+1^*$ never reaches substantial frequency as it is quickly replaced by $2n^*$ in a process similar to *stochastic tunneling*^{20,25}.

158 To test the hypothesis that aneuploidy facilitates adaptation, we estimated F_A , the expected frequency of $2n^*$ that arose from $2n+1$, computed as the average frequency of such $2n_A^*$ cells at the end of
160 simulations using the MAP estimate parameters. Surprisingly, we observe that the majority of $2n^*$

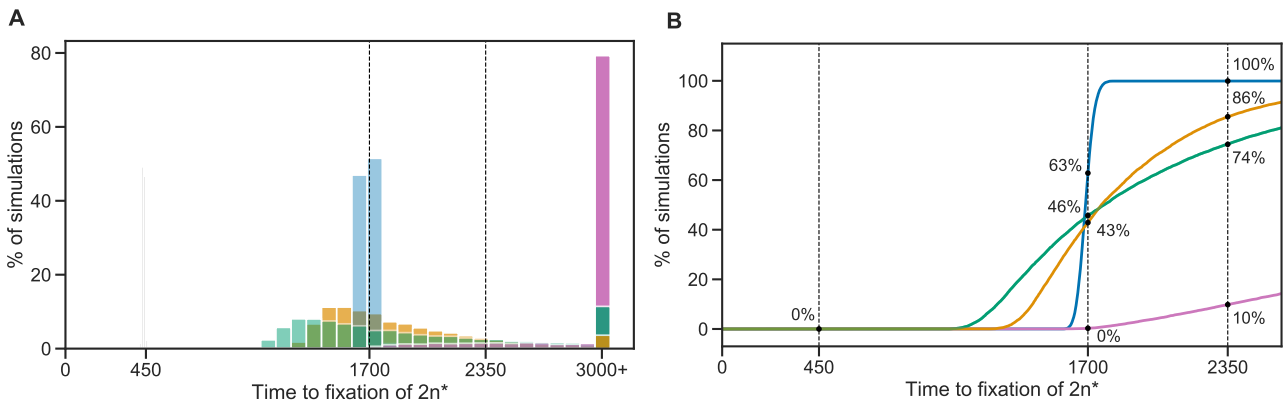


Figure 4: Model fit with and without aneuploidy. The distribution of time to fixation of $2n^*$ (i.e., adaptation time) in 10,000 simulations using MAP parameters of the model with beneficial aneuploidy (blue; $\delta > 0$, $w_{2n} < w_{2n+1} < w_{2n+1^*} < w_{2n^*}$) compared to alternative models: a model with the same parameter values but without aneuploidy (gray, $\delta = 0$, concentrated at $t = 450$); a model fitted to the data assuming no aneuploidy (green, $\delta = 0$); a model fitted to the data assuming neutral aneuploidy (yellow, $\delta > 0$, $w_{2n+1} = w_{2n}$, $w_{2n+1^*} = w_{2n^*}$); and a model with beneficial aneuploidy and an extended prior distribution (pink). In the experiment by Yona et al.⁵⁹, one population lost aneuploidy by generation 1,700 and another by generation 2,350 (dashed lines) but not before generation 450. Thus, the blue distribution has a better fit compared to the other distributions (the gray distribution has a particularly poor fit). The MAP likelihood (eq. (4)) is 0.84, 0.78, 0.67, and 0.14 for the models represented by blue, yellow, green, and pink distributions, respectively. **(A)** Histogram of the time to fixation of $2n^*$. The last bin contains all values equal or greater than 3,000. **(B)** Cumulative distribution of the time to fixation.

cells are $2n_M^*$, a product of a direct mutation in $2n$ cells, rather than descending from $2n+1$ cells

162 ($F_A^{MAP} = 0.106$, average end point of 50 purple lines in Figure 5A). This is despite the fact that the
 $2n+1$ genotype reaches high frequencies in the population (at least 0.98, Figure 5A).

164 This result is not unique to the MAP parameter estimate. We simulated genotype frequency dynamics
 using parameter samples from the posterior distribution, and computed the posterior distribution of F_A
 166 (Figure 5B). The posterior mode F_A was just 0.147 [0.0154-0.370 95% CI] and only in 489 of 100,000
 posterior samples (0.489%) F_A was larger than 0.5 (see Supporting Material for results when transitions
 168 to less-fit genotypes are allowed, such as $2n^*$ to $2n+1^*$). Thus, if we sample a random cell from the
 evolved $2n^*$ population, it is more likely to have descended directly from an euploid cell than from
 170 an aneuploid cell. The probability of $2n^*$ descending from $2n+1$ (F_A) increases with the aneuploidy
 rate, δ , and decreases with both the population size N and the mutation rate, μ (Figure 5C,D). In some
 172 cases it can also be affected by the fitness parameters (Figure S10).

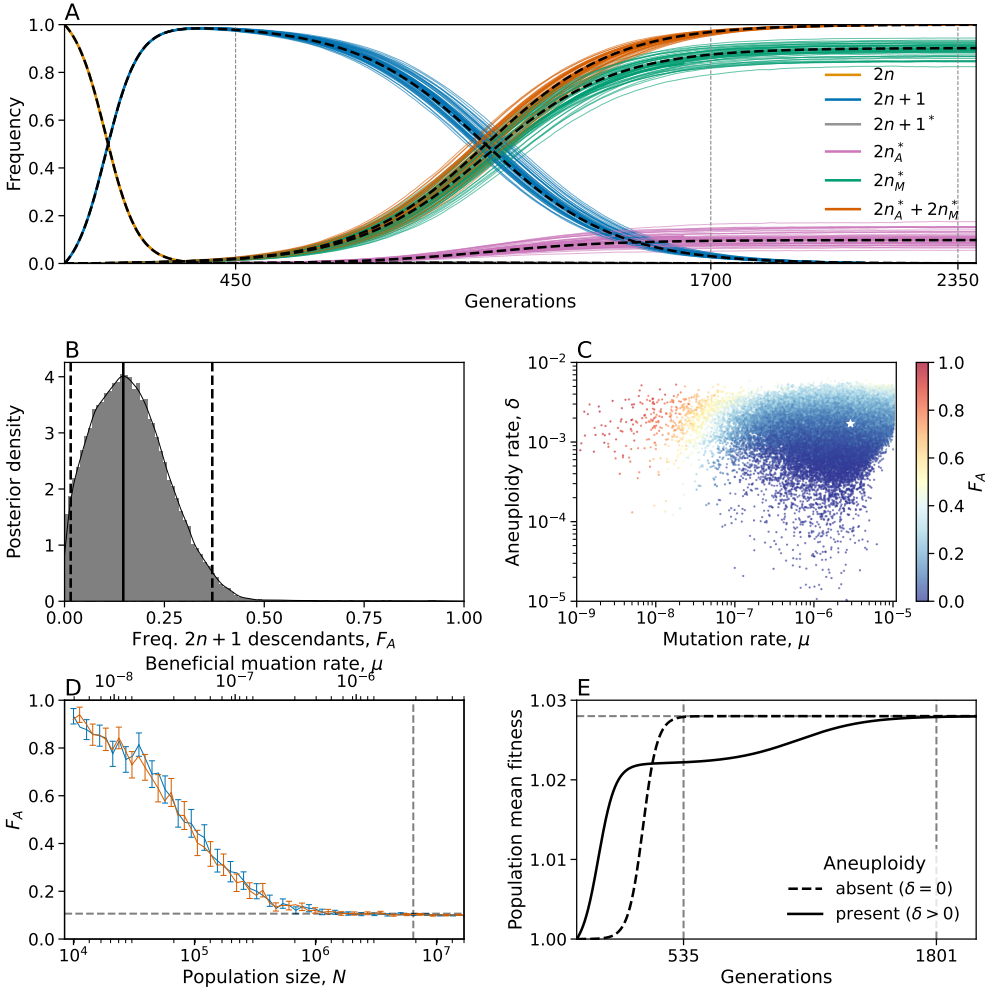


Figure 5: Predicted frequency of aneuploid-descended cells. **(A)** Posterior predicted genotype frequencies over time, including the source of $2n^*$: $2n_A^*$ arose from $2n+1$, whereas $2n_M^*$ arose directly from $2n$. Colored curves are 50 simulations using the MAP estimate parameters. Black dashed curves are the expected genotype frequencies without genetic drift (from a deterministic model). See Figure S9 for log-log scale, in which the sequence of events is easier to observe. **(B)** Posterior distribution of F_A , the expected frequency of $2n^*$ cells descended from $2n+1$ cells, computed as the average frequency at the end of 100 simulations for 100,000 samples from the parameter posterior distribution. Solid and dashed lines show the mode and 95% CI. **(C)** F_A values (color coded) from panel B, with their corresponding mutation rate μ on x-axis and aneuploidy rate δ on the y-axis. White star shows the MAP estimate. See also Figure S10. **(D)** F_A as a function of the population size (N , bottom x-axis) and the beneficial mutation rate (μ , top x-axis) in posterior predictions with MAP parameters. Markers show F_A in 250 simulations per population size or mutation rate value. Error bars show mean F_A with 95% CI (bootstrap, $n = 10,000$). Blue and red bars for varying population size and mutation rate, respectively. Vertical dashed line for population size in the experiment, $6.425 \cdot 10^6$, and the MAP mutation rate, $2.965 \cdot 10^{-6}$. Horizontal line for $F_A^{MAP} = 0.106$. **(E)** Population mean fitness in a model without drift using MAP estimate parameters. Solid lines for mean fitness with aneuploidy ($\delta > 0$), where the population reaches adaptation (mean fitness at 99.99% of maximum value) at generation 1,802. Dashed lines for mean fitness without aneuploidy ($\delta = 0$), where the population adapts much earlier, at generation 535.

Genetic instability in aneuploid cells. It has been suggested that aneuploidy increases genetic instability^{46,19}. Therefore, we inferred model parameters under the assumption that the mutation rate increases in aneuploid cells by a factor $\tau = 1, 33/32$ (due to an additional chromosome), 2, 5, 10, or 100 (due to genetic instability). We found that the posterior distribution was similar for $\tau = 1, 33/32, 2$, and 5 (Figure S4). With $\tau = 100$, the estimated mutation rate was about 7-8-fold lower compared to $\tau = 1$ ($\mu = 4.094 \cdot 10^{-7}$ [$6.252 \cdot 10^{-8} - 6.046 \cdot 10^{-7}$]) and the aneuploidy rate was about 2-3-fold lower ($\delta = 0.744 \cdot 10^{-3}$ [$0.506 \cdot 10^{-3} - 1.827 \cdot 10^{-3}$]). With $\tau = 10$, the estimated mutation rate was only slightly lower compared to $\tau = 1$ ($\mu = 1.67 \cdot 10^{-6}$ [$2.836 \cdot 10^{-8} - 2.245 \cdot 10^{-6}$]). WAIC (lower is better, see Methods) is lowest for $\tau = 33/32$ and $\tau = 1$ (Table S3). Therefore, our results do not support an increase in mutation rate in aneuploid cells. This may be because, unless the increase is strong ($\tau \geq 10$), it does not seem to affect our inference; or because chromosome III is one of the smallest chromosomes¹⁵. We also checked the differences in genotype frequency dynamics for different τ values. We observe $\tau = 100$ could be distinguished if accurate data was available for the waiting time until the frequency of $2n$ to decrease below 95% (Figure S5A) or for waiting time for the frequency of $2n+1$ to either reach or go below 95% (Figure S5B).

188 Discussion

In a landmark study on the role of chromosome duplication in adaptive evolution, Yona et al.⁵⁹ found that a chromosome III trisomy was acquired by *S. cerevisiae* populations evolving under heat stress, only to be later replaced by euploid mutant cells that carry "refined" solutions to the stress. Additionally, such a replacement also occurred when they initiated evolutionary experiments with a population in which all cells carry a chromosome III trisomy. They hypothesized that the euploid mutant cells evolved by heat-resistance mutations in aneuploid cells followed by reversion of trisomy due to a chromosome loss event.

If indeed the evolved euploid population is descended from the aneuploid population, then mutant alleles that were common in the aneuploid populations should also be common in the evolved euploid population. However, we found that this is not the case (Figure 1): mutant allele frequencies in the aneuploid and euploid populations are negatively correlated, such that common alleles in the former are rare in the latter. Furthermore, we developed an evolutionary genetic model of adaptive evolution by aneuploidy and mutation (Figure 2), fitted it to the experimental results of Yona et al.⁵⁹, and used it to predict the genotype frequency dynamics. The model predicted that only about 10-15% of the evolved euploid population descended from aneuploid cells—that is, the majority of the euploid

204 population are not descended from aneuploid cells, but rather are direct descendants of the ancestral
205 wild-type population (Figure 5).

206 This happens despite aneuploidy reaching a high frequency in the population (>95%). Conventional
207 wisdom might suggest that once the aneuploid genotype $2n+1$ reaches high frequency, it will have a
208 better chance at producing "refined" solutions via mutations, and its descendants will come to dominate
209 the population: the frequency of $2n_A^*$ (which arises from $2n+1^*$) will be higher than the frequency of
210 $2n_M^*$ (which arises directly from $2n$).

So how does $2n_M^*$ prevail? Initially, the supply rates of $2n+1$ and $2n_M^*$ are $N\delta \approx 11,000$ and $N\mu \approx 19$,
212 respectively (assuming MAP parameter estimates). Therefore, both genotypes are expected to appear
immediately at the beginning of the experiment (Figure S9). However, $2n+1$ appears at a much higher
214 frequency as $\delta \gg \mu$ by 2-3 orders of magnitude. After they first appear, $2n_M^*$ has higher fitness. But
as long as the frequency of $2n$ is high, the supply rate of $2n+1$ is higher than that of $2n_M^*$, again due to
216 $\delta \gg \mu$. However, supply rates of both genotypes decreases with the frequency of $2n$. Therefore, when
the latter decreases, mainly due to the increase in the frequency of $2n+1$, both supply rates diminish.
218 At this stage, the higher fitness of $2n_M^*$ comes into play and it starts to take over the population,
which is mainly composed of $2n+1$. For the aneuploid lineage to compete with the mutant lineage, it
220 must produce $2n_A^*$ via a mutation followed by chromosome loss. Although this is a stochastic process
(due to drift), our results show that the time until $2n_A^*$ reaches a frequency of 0.1% is roughly 450
222 generations, without much variation (intersection of purple lines and vertical dashed line in Figure S9).
However, by that time $2n_M^*$ is already at a roughly 10-fold higher frequency (1.86%), and since both
224 mutants have the same fitness, their relative frequency remains roughly the same until the end of the
experiment.

226 **Predictions for small populations and low mutation rates.** We examined the effect of the pop-
ulation size, N , and the beneficial mutation rate, μ , on the frequency of $2n+1$ descendants in the
228 evolved population, F_A . We found that F_A is expected to decrease as the population size or mutation
rate increase (Figure 5D), ranging from >90% when the population size is 10,000 or the mutation
230 rate is $6 \cdot 10^{-9}$, to about 10% when the population size is above 1,000,000 (less than the experimental
population size, which was 6,425,000) or the mutation rate is above $2 \cdot 10^{-6}$ (less than the inferred
232 mutation rate, which is $2.965 \cdot 10^{-6}$). Thus, our model provides a testable prediction: if the experiment
was repeated under a lower population size (via stronger daily dilutions or in a smaller volume) or a
234 lower mutation rate (via a non-mutagenic stress or stress with a smaller target size), then the fraction
of the population descending from aneuploid cells would be much higher.

236 **Aneuploidy delays rather than facilitates adaptation.** An additional interesting result of our
study is that aneuploidy increases, rather than decreases, the adaptation time (Figure 5E). This
238 happens despite the fact that the mean fitness initially increases faster in the presence of aneuploidy
(Figure 5E). This is because once $2n+1$ is common, selection for the mutant strain ($2n+1^*$ or $2n^*$) is
240 weaker compared to when $2n^*$ competes directly with $2n$.

242 **Rate and fitness effect of aneuploidy and mutation.** We inferred the rates of aneuploidy and
mutation and their effects on fitness. We estimate that the aneuploidy rate (i.e., number of chromosome
gains per generation) is $1.7 \cdot 10^{-3}$, higher than a previous estimate of $6.7 \cdot 10^{-6}$ (ref⁶²). This may be due
244 to genetic instability caused by heat stress⁵. In addition, we find no evidence for increased mutation
rates in aneuploid cells. Previous empirical studies have suggested that genetic instability (e.g.,
246 elevated mutation rates) in aneuploid cells is due to stress associated with the aneuploid state^{3,6,60,19}.
However, in the experiment of Yona et al.⁵⁹, both the wild-type and the aneuploid were under heat
248 stress, which may explain why we did not find evidence for an increased mutation rate specifically in
aneuploid cells.

250 **Conclusions.** Here, we tested the hypothesis that aneuploid cells are an evolutionary "stepping
stone", or adaptive intermediate, between wild-type euploid cells and mutant euploid cells. Our
252 results suggest that, although it seems the population goes from euploid to aneuploid and back, this is
not the case at the individual level. We estimate that only about 10-15% of the euploid cells descended
254 from aneuploid cells, whereas the rest are direct descendants of the wild-type euploid cells. Thus,
aneuploidy can delay, rather than accelerate, adaptation, and cells that become aneuploid may
256 leave less descendants than cells that remain euploid. This surprising result reinforces the importance
of models when making interpretations on evolutionary processes, and emphasizes the unintuitive
258 outcomes of clonal interference during adaptive evolution.

Models and Methods

260 **DNA sequencing.** Whole-genome sequencing of the ancestral diploid strain ($2n$) was performed
on a single colony of the ancestor. Whole-genome sequencing of the four evolving populations ($H2$
262 after 450 and 2,350 generations, and $H4$ after 450 and 1,700 generations) was performed on a sample
from these populations (rather than from single colonies) in order to maintain the population diversity.
264 Cells were grown in 5ml of YPD medium, either at 30 °C (ancestral diploid) or 39 °C (evolved

populations) in shaking conditions (200rpm) until reaching stationary phase. Following growth, 3ml
 266 of each culture were centrifuge (14,000rpm) and cell pellets were used for DNA extraction. Genomic
 DNA was extracted using $\text{A}\ddot{\text{I}}\text{JMasterPure Yeast DNA Purification Kit}$ (Lucigen) according to the
 268 manufacture instructions. Following extraction, DNA concentrations were determined by Qubit assay
 (Thermo Fisher) and $1\text{ }\text{\AA}\text{g}$ DNA was used for library preparation using Illumina sample preparation
 270 kit (Illumina). Samples were sequenced using a 100 bp pair end read output run using Illumina
 HiSeq2500.

272 **Evolutionary genetic model.** We model the evolution of a population of cells using a Wright-Fisher
 model³², assuming a constant effective population size N , non-overlapping generations, and including
 274 the effects of natural selection, genetic drift, aneuploidy, and mutation. We focus on beneficial genetic
 modifications, neglecting the effects of deleterious and neutral mutations or karyotypic changes. The
 276 model allows for a single aneuploid karyotype (e.g., chromosome III duplication) and a single mutation
 to accumulate in the genotype. Thus, the model follows four genotypes (Figure 2): euploid wild-type,
 278 $2n$, the initial genotype; euploid mutant, $2n^*$, with the standard karyotype and a single beneficial muta-
 tion; aneuploid wild-type, $2n+1$, with an extra chromosome, i.e., following chromosome duplication;
 280 and aneuploid mutant, $2n+1^*$, with and extra chromosome and a beneficial mutation.

Transitions between the genotypes occur as follows (Figure 2): Beneficial mutations from $2n$ to $2n^*$
 282 and from $2n+1$ to $2n+1^*$ occur with probability μ , the mutation rate. We neglect back-mutations (i.e.,
 from $2n^*$ to $2n$ and from $2n+1^*$ to $2n+1$). Aneuploidy is formed by chromosome mis-segregation,
 284 so that cells transition from $2n$ to $2n+1$ and from $2n+1^*$ to $2n^*$ with probability δ , the aneuploidy
 rate. That is, we assume chromosomes are gained and lost at the same rate, and we neglect events that
 286 form a less-fit genotype (i.e., $2n+1$ to $2n$ and $2n^*$ to $2n+1^*$).

In the experiment by Yona et al.⁵⁹, the population was grown every day from $1.6 \cdot 10^6$ cells until
 288 reaching stationary phase and then diluted 1:120. Thus, we set the population size to $N = 6.425 \cdot 10^6$,
 the harmonic mean of $\{2^k \cdot 1.6 \cdot 10^6\}_{k=0}^7$ ⁹. The initial population has N cells with genotype $2n$. The
 290 effect of natural selection on the frequency f_i of genotype $i = 2n, 2n + 1, 2n + 1^*,$ or $2n^*$ is given
 by

$$292 \quad f_i^s = \frac{f_i w_i}{\bar{w}}, \quad (1)$$

where w_i is the fitness of genotype i and $\bar{w} = \sum_j f_j w_j$ is the population mean fitness. The effect of

294 mutation and aneuploidy on genotype frequencies is given by

$$\begin{aligned} f_{2n}^m &= (1 - \delta - \mu)f_{2n}^s, \\ f_{2n+1}^m &= \delta f_{2n}^s + (1 - \mu)f_{2n+1}^s, \\ f_{2n+1^*}^m &= \mu f_{2n+1}^s + (1 - \delta)f_{2n+1^*}^s, \\ f_{2n^*}^m &= \mu f_{2n}^s + \delta f_{2n+1}^s + f_{2n^*}^s. \end{aligned} \tag{2}$$

296 Finally, random genetic drift is modeled using a multinomial distribution³²,

$$\mathbf{f}' \sim \frac{1}{N} \cdot \text{Mult}(N, \mathbf{f}^m), \tag{3}$$

298 where $\mathbf{f}^m = (f_{2n}^m, f_{2n+1}^m, f_{2n+1^*}^m, f_{2n^*}^m)$ are the frequencies of the genotypes after mutation and
aneuploidy, \mathbf{f}' are the genotype frequencies in the next generation, and $\text{Mult}(N, \mathbf{f})$ is a multinomial
300 distribution parameterized by the population size N and the genotype frequencies \mathbf{f} . Overall, the change
in genotype frequencies from one generation to the next is given by the transformation $f_i \rightarrow f'_i$.

302 **Empirical data for model inference.** We use the results of evolutionary experiments reported by
Yona et al.⁵⁹. In their heat-stress experiment, four populations of *S. cerevisiae* evolved under 39 °C.
304 Aneuploidy fixed in all four population in the first 450 generations. Hereafter, fixation or elimination
of a genotype *by generation t* means that more than 95% or less than 5% of the population carry the
306 genotype at generation t , and possibly earlier. From re-analysis of data not published in the original
paper, aneuploidy did not fix before at least 200 generations elapsed. The experiment continued with
308 two populations, in which aneuploidy was eliminated by generation 1,700 and 2,350 while still under
the same conditions of elevated heat (39 °C).

310 **Likelihood function.** Because our model, just like the Wright-Fisher model, is non-linear and
stochastic, computing the distribution of fixation time $T(g)$ of genotype g for use in the likelihood
312 function is intractable (it is even hard to use a diffusion-equation approximation due to the model having
multiple genotypes, rather than just two). We overcome this problem by approximating the likelihood
314 using simulations. We simulate 1,000 experiments per parameter vector $\theta = (\mu, \delta, s, b, c)$, resulting in
a set of simulated observations $\tilde{\mathbf{X}} = \{\tilde{X}_i\}_{i=1}^{1000}$. We then compute the approximate likelihood,

$$\begin{aligned} \mathcal{L}(\theta) &= P^4(200 \leq T(2n+1) \leq 450) \cdot \left[1 - \right. \\ &\quad P_{\tilde{\mathbf{X}}}^4(\{T(2n^*) < 1700\} \mid 200 \leq T(2n+1) \leq 450) - \\ &\quad P_{\tilde{\mathbf{X}}}^4(\{1700 < T(2n^*) < 2350\} \mid 200 \leq T(2n+1) \leq 450) + \\ &\quad \left. P_{\tilde{\mathbf{X}}}^4(\{T(2n^*) < 1700\} \wedge \{1700 < T(2n^*) < 2350\} \mid 200 \leq T(2n+1) \leq 450) \right], \end{aligned} \tag{4}$$

316

where $!\{\dots\}$ is the "logical not" operator, $P^4(\dots)$ is the 4th power of $P(\dots)$, and all probabilities $P_{\tilde{\mathbf{X}}}(\dots)$ are approximated from the results of the simulations $\tilde{\mathbf{X}}$. For example, $P_{\tilde{\mathbf{X}}}(!\{T(2n^*) < 1700\} \mid 200 \leq T(2n+1) \leq 450)$ is approximated by taking simulations in which $2n+1$ fixed before generation 450 but not before generation 200, and computing the fraction of such simulations in which $2n^*$ did not fix by generation 1,700, and hence aneuploidy did not extinct before generation 1,700. Figure S1 compares results with less and more simulated experiments, demonstrating that 1,000 simulations are likely sufficient.

For a model without aneuploidy (that is, when the aneuploidy rate is fixed at zero, $\delta = 0$), we disregard the increased expression in chromosome III and the growth advantage measured in generation 450, and focus on the growth advantage measured in later generations, presumably due to a beneficial mutation. Therefore, the likelihood is approximated by

$$\begin{aligned} \mathcal{L}_!(\theta) = 1 - P_{\tilde{\mathbf{X}}}^4(!\{T(2n^*) < 1700\}) - \\ P_{\tilde{\mathbf{X}}}^4(!\{1700 < T(2n^*) < 2350\}) + \\ P_{\tilde{\mathbf{X}}}^4(!\{T(2n^*) < 1700\} \wedge !\{1700 < T(2n^*) < 2350\}) . \end{aligned} \quad (5)$$

Parameter inference. To infer model parameters, we use approximate Bayesian computation with a sequential Monte-Carlo scheme, or ABC-SMC⁴⁹, implemented in the `pyABC` Python package²⁴ pyabc.readthedocs.io. This approach uses numerical stochastic simulations of the model to infer a posterior distribution over the model parameters. It is a method of likelihood-free, simulation-based inference⁸, that is, for estimating a posterior distribution when a likelihood function cannot be directly computed. It is therefore suitable in our case, in which the likelihood function can only be approximated from simulations, and cannot be directly computed.

The ABC-SMC algorithm employs sequential importance sampling over multiple iterations^{52,23,50}. In iteration t of the algorithm, a set of parameter vectors, $\{\theta_{i,t}\}_{i=1}^{n_t}$, also called *particles*, are constructed in the following way. A proposal particle, θ^* , is sampled from a proposal distribution, and is either accepted or rejected, until n_t particles are accepted. The number of particles, n_t , is adapted at every iteration t using the adaptive population strategy²⁴ pyabc.readthedocs.io. For $t = 0$, the proposal particle is sampled from the prior distribution, $p(\theta)$. For $t > 0$, the proposal particle is sampled from the particles accepted in the previous iteration, $\{\theta_{i,t-1}\}_{i=1}^{n_{t-1}}$, each with a probability relative to its weight $W_{t-1}(\theta_{i,t-1})$ (see below). The proposal particle is then perturbed using a kernel perturbation kernel, $K_t(\theta^* \mid \theta)$ where θ is the sample from the previous iteration. Then, a set of synthetic observations $\tilde{\mathbf{X}}^*$ is simulated, and the proposal particle θ^* is accepted if its approximate likelihood (eq. (4)) is high enough, $\mathcal{L}(\theta^*) > 1 - \epsilon_t$ (or more commonly, if $1 - \mathcal{L}(\theta^*) < \epsilon_t$), where $\epsilon_t > 0$ is the *acceptance*

threshold, as higher values of ϵ_t allow more particles to be accepted. The acceptance threshold ϵ_t is chosen as the median of the $1 - \mathcal{L}(\theta)$ of the particles accepted in the previous iteration, $t - 1$, and $\epsilon_0 = 0.01$. For each accepted particle $\theta_{i,t}$ a weight $W_t(\theta_{i,t})$ is assigned: for $t = 0$, $W_0(\theta_{i,0}) = 1$, and for $t > 0$, $W_t(\theta_{i,t}) = p(\theta_{i,t}) / \sum_{i=1}^{n_{t-1}} W_{t-1}(\theta_{i,t-1}) K_t(\theta_{i,t}, \theta_{i,t-1})$, where $p(\theta)$ is the prior density of θ and $K_t(\theta', \theta)$ is the probability of a perturbation from θ to θ' . $K_t(\theta' | \theta)$ is a multivariate normal distribution, fitted at iteration t to the particles from the previous iteration, $\{\theta_{i,t-1}\}_{i=1}^{n_{t-1}}$, and their weights, $\{W(\theta_{i,t-1})\}_{i=1}^{n_{t-1}}$.

Acceptance is determined according to the approximate likelihood (eq. (4)), which has a maximum value of $\mathcal{L}_{max} = 0.875$ (giving a minimal value of $\epsilon_{min} = 0.125$). We terminated the inference iterations when the change in ϵ value from one iteration to the next was small. With our standard prior and model, we reached $\epsilon = 0.13$ (or $\mathcal{L} = 0.87$) after six iterations, with $n_6 = 982$ accepted parameter vectors and effective sample size ESS=651 (Figure S2). Running the inference algorithm with different initialization seeds and less or more simulations for approximating the likelihood produced similar posterior distributions (Figure S1).

After producing a set of weighted particles from the the posterior distribution using the above ABC-SMC algorithm, we approximate the posterior using kernel density estimation (KDE) with Gaussian kernels. We truncate the estimated posterior to avoid positive posterior density for values with zero prior density. The MAP (maximum a posteriori) estimate is computed as the the maximum of the estimated joint posterior density. We then draw 5,000,000 samples from the posterior distribution to compute the HDI (highest density interval) and draw 50,000 samples to visualize the posterior distribution with histograms.

Model comparison. We examine several versions of our evolutionary models, e.g. without aneuploidy or with increased mutation rate in aneuploid cells, as well as several different prior distributions (see below). To compare these, we plot posterior predictions: for each model we execute 10,000 simulations using the MAP parameter estimates and plot the distributions of time to fixation of $2n^*$, one of key properties of the model likelihood. These plots visualize the fit of each model to the data. Also, for similar models we plot the marginal and joint posterior distributions of the parameters; if these are similar, we consider the models interchangeable. We validate this by comparing HDI (highest density interval) of posterior distributions.

Where posterior plots are very similar and the number of parameters is the same, we use WAIC, or

the widely applicable information criterion¹², defined as

378 $WAIC(\theta) = -2 \log \mathbb{E}[\mathcal{L}(\theta)] + 2\mathbb{V}[\log \mathcal{L}(\theta)]$ (6)

where θ is a parameter vector, and $\mathbb{E}[\cdot]$ and $\mathbb{V}[\cdot]$ are the expectation and variance taken over the posterior distribution, which in practice are approximated using 50,000 samples from the posterior KDE. We validated that upon resampling WAIC values do not significantly change and that differences in WAIC between models are preserved. WAIC values are scaled as a deviance measure: lower values imply higher predictive accuracy²¹.

384 **Prior distributions.** We used informative prior distributions for $w_{2n+1} = 1 - c + b$, $w_{2n+1^*} = (1+s)(1-c)+b$ and $w_{2n^*} = 1+s$, which we estimated from growth curves data from mono-culture growth experiments previously reported by Yona et al.⁵⁹, Figs. 3C, 4A, and S2. We used Curveball, a method for predicting results of competition experiments from growth curve data³⁵ curveball.yoavram.com.

388 Briefly, Curveball takes growth curves of two strains growing separately in mono-culture and predicts how they would grow in a mixed culture, that is, it predicts the results of a competition assay. From these predictions, relative fitness values can be computed. Because Curveball uses a maximum-likelihood approach to estimate model parameters, we were able to estimate a distribution of relative fitness values to be used as a prior distribution by sampling 10,000 samples from a truncated multivariate normal distribution defined by the maximum-likelihood covariance matrix (Figure S3).

394 We used growth curves of $2n$ and $2n+1$ in 39 °C to estimate an informative prior distribution for w_{2n+1} (Figure S3-D, assuming $w_{2n} = 1$). In this prior distribution, we used the same prior for w_{2n+1^*} and w_{2n^*} . To increase computational efficiency, we also assumed $w_{2n^*} > w_{2n+1^*} > w_{2n+1} > w_{2n}$; running the inference without this assumption produced similar results. See *supporting material* for 398 an extended informative prior distribution that uses growth curves of $2n^*$ and $2n+1$ growing in 39 °C; this prior distribution proved to be less useful.

400 As a control, we tested an uninformative uniform prior with $U(1, 6)$, for (i) all w_{2n+1} , w_{2n+1^*} , w_{2n^*} , or (ii) only for w_{2n+1^*} , w_{2n^*} , using the above informative prior for w_{2n+1} . In these cases the inference 402 algorithm failed to converge.

For the mutation rate, μ , and aneuploidy rate, δ , we used uninformative uniform priors, $\mu \sim U(10^{-9}, 10^{-5})$ and $\delta \sim U(10^{-6}, 10^{-2})$. A wider mutation rate prior, $\mu \sim U(10^{-9}, 10^{-3})$, produced similar results.

406 Acknowledgements

We thank Lilach Hadany, Judith Berman, David Gresham, Shay Covo, Martin Kupiec, Uri Obolski, Daniel
408 Weissman, and Tal Simon for discussions and comments. This work was supported in part by the Israel Science
Foundation (ISF, YR 552/19), the US–Israel Binational Science Foundation (BSF, YR 2021276) Minerva
410 Stiftung center for Lab Evolution (YR), Minerva Stiftung short-term research grant (MP).

References

- 412 [1] Avecilla, G., Chuong, J. N., Li, F., Sherlock, G., Gresham, D. and Ram, Y. 2022, ‘Neural
networks enable efficient and accurate simulation-based inference of evolutionary parameters
414 from adaptation dynamics’, *PLOS Biology* **20**(5), e3001633.
- [2] Bakhoum, S. F. and Landau, D. A. 2017, ‘Chromosomal instability as a driver of tumor hetero-
416 geneity and evolution’, *Cold Spring Harb. Perspect. Med.* **7**(6), 1–14.
- [3] Bouchonville, K., Forche, A., Tang, K. E. S., Semple, C. a. M. and Berman, J. 2009, ‘Aneuploid
418 chromosomes are highly unstable during dna transformation of *Candida albicans*’, *Eukaryot.
Cell* **8**(10), 1554–66.
- 420 [4] Boveri, T. 2008, ‘Concerning the origin of malignant tumours’, *J. Cell Sci.* **121**(Supplement
1), 1–84.
- 422 [5] Chen, G., Bradford, W. D., Seidel, C. W. and Li, R. 2012, ‘Hsp90 stress potentiates rapid cellular
adaptation through induction of aneuploidy.’, *Nature* **482**(7384), 246–50.
- 424 [6] Chen, G., Rubinstein, B. and Li, R. 2012, ‘Whole chromosome aneuploidy: Big mutations drive
adaptation by phenotypic leap’, *BioEssays* **34**(10), 893–900.
- 426 [7] Covo, S., Puccia, C. M., Argueso, J. L., Gordenin, D. A. and Resnick, M. A. 2014, ‘The sister
chromatid cohesion pathway suppresses multiple chromosome gain and chromosome amplifica-
428 tion.’, *Genetics* **196**(2), 373–384.
- [8] Cranmer, K., Brehmer, J. and Louppe, G. 2020, ‘The frontier of simulation-based inference’,
430 *Proceedings of the National Academy of Sciences* p. 201912789.
- [9] Crow, J. F. and Kimura, M. 1970, *An introduction to population genetics theory*, Burgess Pub.
432 Co., Minneapolis.

- [10] Dhar, R. and Sägesser, R and Weikert, C and Yuan, J and Wagner, Andreas, doi = 10.1111/j.1420-9101.2011.02249.x, i . . j. . J. m. . m. n. . p. . p. . t. . A. v. . y. . n.d..
- [11] Dunham, M. J., Badrane, H., Ferea, T., Adams, J., Brown, P. O., Rosenzweig, F. and Botstein, D. 2002, ‘Characteristic genome rearrangements in experimental evolution of *Saccharomyces cerevisiae*’, *Proc. Natl. Acad. Sci.* **99**(25), 16144–16149.
- [12] Gelman, A., Carlin, J. B., Stern, H. S., Dunson, D. B., Vehtari, A. and Rubin, D. B. 2013, *Bayesian Data Analysis, Third Edition*, Chapman & Hall/CRC Texts in Statistical Science, Taylor & Francis.
- [13] Gerstein, A. C. and Berman, J. 2018, ‘Diversity of acquired adaptation to fluconazole is influenced by genetic background and ancestral fitness in *Candida albicans*’, *bioRxiv* p. 360347.
- [14] Gerstein, A. C., Ono, J., Lo, D. S., Campbell, M. L., Kuzmin, A. and Otto, S. P. 2015, ‘Too much of a good thing: the unique and repeated paths toward copper adaptation.’, *Genetics* **199**(2), 555–71.
- [15] Gilchrist, C. and Stelkens, R. 2019, ‘Aneuploidy in yeast: Segregation error or adaptation mechanism?’, *Yeast* **36**(9), 525–539.
- [16] Gresham, D., Desai, M. M., Tucker, C. M., Jenq, H. T., Pai, D. A., Ward, A., DeSevo, C. G., Botstein, D. and Dunham, M. J. 2008, ‘The repertoire and dynamics of evolutionary adaptations to controlled nutrient-limited environments in yeast’, *PLoS Genet.* **4**(12).
- [17] Heidenreich, E. 2007, ‘Adaptive Mutation in *< i>Saccharomyces cerevisiae</i>*’, *Crit. Rev. Biochem. Mol. Biol.* **42**(4), 285–311.
- [18] Hong, J. and Gresham, D. 2014, ‘Molecular specificity, convergence and constraint shape adaptive evolution in nutrient-poor environments’, *PLoS Genet.* **10**(1).
- [19] Ippolito, M. R., Martis, V., Martin, S., Tijhuis, A. E., Hong, C., Wardenaar, R., Dumont, M., Zerbib, J., Spierings, D. C., Fachinetti, D., Ben-David, U., Foijer, F. and Santaguida, S. 2021, ‘Gene copy-number changes and chromosomal instability induced by aneuploidy confer resistance to chemotherapy’, *Dev. Cell* **56**(17), 2440–2454.e6.
- [20] Iwasa, Y., Michor, F. and Nowak, M. A. 2004, ‘Stochastic tunnels in evolutionary dynamics’, *Genetics* **166**(3), 1571–1579.
- [21] Kass, R. E. and Raftery, A. E. 1995, ‘Bayes factors’, *J. Am. Stat. Assoc.* **90**(430), 773.
- [22] Kasuga, T., Bui, M., Bernhardt, E., Swiecki, T., Aram, K., Cano, L. M., Webber, J., Brasier,

- C., Press, C. and Grünwald, Niklaus J. and Rizzo, David M. and Garbelotto, Matteo, doi
464 = 10.1186/s12864-016-2717-z, i...i...j..B.n...p...p...p..B.t..H.v...y...n.d..
- [23] Klinger, E. and Hasenauer, J. 2017, A scheme for adaptive selection of population sizes in
466 approximate bayesian computation - sequential monte carlo, *in* J. Feret and H. Koepll, eds,
‘Computational Methods in Systems Biology’, Vol. 10545, Springer International Publishing,
468 pp. 128–144. Series Title: Lecture Notes in Computer Science.
- [24] Klinger, E., Rickert, D. and Hasenauer, J. 2018, ‘pyabc: distributed, likelihood-free inference’,
470 *Bioinformatics* (May), 1–3.
- [25] Komarova, N. L., Sengupta, A. and Nowak, M. A. 2003, ‘Mutation-selection networks of cancer
472 initiation: Tumor suppressor genes and chromosomal instability’, *J. Theor. Biol.* **223**(4), 433–
450.
- [26] Kumaran, R., Yang, S.-Y. and Leu, J.-Y. n.d., ‘Characterization of chromosome stability in
474 diploid, polyploid and hybrid yeast cells’, **8**(7), e68094.
- [27] Lynch, M., Sung, W., Morris, K., Coffey, N., Landry, C. R., Dopman, E. B., Dickinson, W. J.,
Okamoto, K., Kulkarni, S., Hartl, D. L. and Thomas, W. K. 2008, ‘A genome-wide view of the
478 spectrum of spontaneous mutations in yeast’, *Proceedings of the National Academy of Sciences*
105(27), 9272–9277.
- [28] Mannaert, A., Downing, T., Imamura, H. and Dujardin, J. C. 2012, ‘Adaptive mechanisms in
480 pathogens: Universal aneuploidy in *Leishmania*’, *Trends Parasitol.* **28**(9), 370–376.
- [29] Möller, M., Habig, M., Freitag, M. and Stukenbrock, E. H. 2018, ‘Extraordinary genome
482 instability and widespread chromosome rearrangements during vegetative growth’, *Genetics*
210(2), 517–529.
- [30] Naylor, R. M. and van Deursen, J. M. 2016, ‘Aneuploidy in cancer and aging’, *Annu. Rev. Genet.*
486 **50**(1), 45–66.
- [31] Niwa, O., Tange, Y. and Kurabayashi, A. 2006, ‘Growth arrest and chromosome instability in
488 aneuploid yeast’, *Yeast* **23**(13), 937–950.
- [32] Otto, S. P. and Day, T. 2007, *A biologist’s guide to mathematical modeling in ecology and*
490 *evolution*, Princeton University Press.
- [33] Pavelka, N., Rancati, G., Zhu, J., Bradford, W. D., Saraf, A., Florens, L., Sanderson, B. W., Hat-

- 492 tem, G. L. and Li, R. 2010, ‘Aneuploidy confers quantitative proteome changes and phenotypic variation in budding yeast.’, *Nature* **468**(7321), 321–5.
- 494 [34] Peter, J., De Chiara, M., Friedrich, A., Yue, J. X., Pflieger, D., Bergström, A., Sigwalt, A., Barre, B., Freel, K., Llored, A., Cruaud, C., Labadie, K., Aury, J. M., Istance, B., Lebrigand, K., Barbry, P., Engelen, S., Lemainque, A., Wincker, P., Liti, G. and Schacherer, J. 2018, ‘Genome evolution across 1,011 *< i>Saccharomyces cerevisiae</i>* isolates’, *Nature* **556**(7701), 339–344.
- 496 498 [35] Ram, Y., Dellus-Gur, E., Bibi, M., Karkare, K., Obolski, U., Feldman, M. W., Cooper, T. F., Berman, J. and Hadany, L. 2019, ‘Predicting microbial growth in a mixed culture from growth curve data’, *Proceedings of the National Academy of Sciences* **116**(29), 14698–14707.
- 500 502 [36] Rancati, G., Pavelka, N., Fleharty, B., Noll, A., Trimble, R., Walton, K., Perera, A., Staehling-Hampton, K., Seidel, C. W. and Li, R. 2008, ‘Aneuploidy underlies rapid adaptive evolution of yeast cells deprived of a conserved cytokinesis motor’, *Cell* **135**(5), 879–893.
- 504 [37] Robbins, N., Caplan, T. and Cowen, L. E. 2017, ‘Molecular evolution of antifungal drug resistance’, *Annu. Rev. Microbiol.* **71**(1), 753–775.
- 506 [38] Rodrigues, M. L. and Albuquerque, P. C. 2018, ‘Searching for a change: The need for increased support for public health and research on fungal diseases’, *PLoS Negl. Trop. Dis.* **12**(6), 1–5.
- 508 [39] Santaguida, S. and Amon, A. 2015, ‘Short- and long-term effects of chromosome mis-segregation and aneuploidy’, *Nat. Rev. Mol. Cell Biol.* **16**(8), 473–485.
- 510 [40] Santaguida, S., Vasile, E., White, E. and Amon, A. 2015, ‘Aneuploidy-induced cellular stresses limit autophagic degradation’, *Genes Dev.* **29**(19), 2010–2021.
- 512 [41] Schwartzman, J. M., Sotillo, R. and Benezra, R. 2010, ‘Mitotic chromosomal instability and cancer: Mouse modelling of the human disease’, *Nat. Rev. Cancer* **10**(2), 102–115.
- 514 [42] Selmecki, A. M., Dulmage, K., Cowen, L. E., Anderson, J. B. and Berman, J. 2009, ‘Acquisition of aneuploidy provides increased fitness during the evolution of antifungal drug resistance’, *PLoS Genet.* **5**(10), e1000705.
- 516 518 [43] Selmecki, A. M., Forche, A. and Berman, J. 2010, ‘Genomic plasticity of the human fungal pathogen *Candida albicans*’, *Eukaryot. Cell* **9**(7), 991–1008.
- 520 [44] Selmecki, A. M., Gerami-Nejad, M., Paulson, C., Forche, A. and Berman, J. 2008, ‘An isochromosome confers drug resistance in vivo by amplification of two genes, erg11 and tac1’, *Mol. Microbiol.* **68**(3), 624–641.

- 522 [45] Sheltzer, J. M. and Amon, A. 2011, ‘The aneuploidy paradox: Costs and benefits of an incorrect
karyotype’, *Trends Genet.* **27**(11), 446–453.
- 524 [46] Sheltzer, J. M., Blank, H. M., Pfau, S. J., Tange, Y., George, B. M., Humpton, T. J., Brito, I. L.,
Hiraoka, Y., Niwa, O. and Amon, A. 2011, ‘Aneuploidy drives genomic instability in yeast’,
526 *Science* **333**(6045), 1026–1030.
- 528 [47] Sheltzer, J. M., Ko, J. H., Replogle, J. M., Habibe Burgos, N. C., Chung, E. S., Meehl, C. M.,
Sayles, N. M., Passerini, V., Storchova, Z. and Amon, A. 2017, ‘Single-chromosome gains
commonly function as tumor suppressors’, *Cancer Cell* **31**(2), 240–255.
- 530 [48] Sionov, E., Lee, H., Chang, Y. C. and Kwon-Chung, K. J. 2010, ‘*Cryptococcus neoformans*
overcomes stress of azole drugs by formation of disomy in specific multiple chromosomes’,
532 *PLoS Pathog.* **6**(4), e1000848.
- 534 [49] Sisson, S. A., Fan, Y. and Tanaka, M. M. 2007, ‘Sequential monte carlo without likelihoods’,
Proceedings of the National Academy of Sciences **104**(6), 1760–1765.
- 536 [50] Syga, S., David-Rus, D. and Schälte, Yannik and Hatzikirou, Haralampos and Deutsch, Andreas,
doi = 10.1038/s41598-021-01407-y, j. . S. n. . p. . t. . I. v. . y. . n.d..
- 538 [51] Todd, R. T., Forche, A. and Selmecki, A. M. 2017, ‘Ploidy variation in fungi: Polyploidy,
aneuploidy, and genome evolution’, *Microbiol. Spectr.* **5**(4), 1–20.
- 540 [52] Toni, T., Welch, D., Strelkowa, N., Ipsen, A. and Stumpf, M. P. 2009, ‘Approximate bayesian
computation scheme for parameter inference and model selection in dynamical systems’, *J. R.
Soc. Interface* **6**(31), 187–202.
- 542 [53] Torres, E. M., Dephoure, N., Panneerselvam, A., Tucker, C. M., Whittaker, C. A., Gygi, S. P.,
Dunham, M. J. and Amon, A. 2010, ‘Identification of aneuploidy-tolerating mutations’, *Cell*
544 **143**(1), 71–83.
- 546 [54] Torres, E. M., Sokolsky, T., Tucker, C. M., Chan, L. Y., Boselli, M., Dunham, M. J. and Amon,
A. 2007, ‘Effects of aneuploidy on cellular physiology and cell division in haploid yeast’, *Science*
(80-.). **317**(5840), 916–924.
- 548 [55] Tsai, H. J., Nelliat, A. R., Choudhury, M. I., Kucharavy, A., Bradford, W. D., Cook, M. E., Kim,
J., Mair, D. B., Sun, S. X., Schatz, M. C. and Li, R. 2019, ‘Hypo-osmotic-like stress underlies
550 general cellular defects of aneuploidy’, *Nature* .
- [56] Williams, B. R., Prabhu, V. R., Hunter, K. E., Glazier, C. M., Whittaker, C. a., Housman,

- 552 D. E. and Amon, A. 2008, ‘Aneuploidy affects proliferation and spontaneous immortalization in
mammalian cells’, *Science* **322**(5902), 703–709.
- 554 [57] Yang, F., Todd, R. T., Selmecki, A., Jiang, Y. Y., Cao, Y. B. and Berman, J. 2021, ‘The fitness
costs and benefits of trisomy of each *Candida albicans* chromosome’, *Genetics* **218**(2), 1–7.
- 556 [58] Yona, A. H., Frumkin, I. and Pilpel, Y. 2015, ‘A relay race on the evolutionary adaptation
spectrum’, *Cell* **163**(3), 549–559.
- 558 [59] Yona, A. H., Manor, Y. S., Herbst, R. H., Romano, G. H., Mitchell, A., Kupiec, M., Pilpel, Y.
and Dahan, O. 2012, ‘Chromosomal duplication is a transient evolutionary solution to stress.’,
560 *Proceedings of the National Academy of Sciences* **109**(51), 21010–5.
- 562 [60] Zhu, J., Pavelka, N., Bradford, W. D., Rancati, G. and Li, R. 2012, ‘Karyotypic determinants of
chromosome instability in aneuploid budding yeast’, *PLoS Genetics* **8**(5).
- 564 [61] Zhu, J., Tsai, H.-J., Gordon, M. R. and Li, R. 2018, ‘Cellular stress associated with aneuploidy’,
Dev. Cell **44**(4), 420–431.
- 566 [62] Zhu, Y. O., Sherlock, G. and Petrov, D. A. 2016, ‘Whole genome analysis of 132 clinical *Sac-*
charomyces cerevisiae strains reveals extensive ploidy variation’, *G3 Genes, Genomes, Genetics*
6(8), 2421–2434.
- 568 [63] Zhu, Y. O., Siegal, M. L., Hall, D. W. and Petrov, D. A. 2014, ‘Precise estimates of mutation rate
and spectrum in yeast’, *Proceedings of the National Academy of Sciences* **111**(22), E2310–E2318.

570 Supplementary Material

Supplementary Analysis

572 **Sensitivity analysis.** Changing a single parameter while keeping the rest fixed at the MAP estimate produces a worse fit to the data (Figure S6). Furthermore, we fitted models with a mutation rate
574 fixed at $\mu = 10^{-5}$, 10^{-6} and 10^{-7} . We inferred similar parameters estimates for the model with
576 $\mu = 10^{-6}$ compared to the model with a free μ parameter, in which the inferred mutation rate is
578 $\mu \approx 3 \cdot 10^{-6}$. Inference assuming $\mu = 10^{-5}$ or $\mu = 10^{-7}$ produced similar estimates except that the estimated aneuploidy rate, δ , was higher, and assuming $\mu = 10^{-7}$, the estimated fitness of $2n+1$ was lower (Figure S7).

580 **Extended informative prior distribution.** In an extended informative prior distribution, we used additional growth curves of $2n^*$ (*refined* strain from Yona et al.⁵⁹) and $2n+1$ in 39 °C to estimate
582 w_{2n^*}/w_{2n+1} (Figure S3L). The same distribution was used for w_{2n^*}/w_{2n+1*} . Thus, our main informative prior uses a single prior distribution for fitness values of $2n+1$, $2n+1^*$, and $2n^*$, whereas the extended informative prior uses one distribution for $2n+1$, and another distribution for both $2n+1^*$
584 and $2n^*$.

586 We estimated the parameters under this extended informative prior. Inference took much longer to run but the posterior distribution seemed to converge, as it did not change much in the final iterations. The posterior predictive plot shows that inference with this extended prior produces a
588 posterior distribution that fails to explain the empirical observations (pink in Figure 4). However, the inferred posterior distribution is considerably narrower (compare Figures 3 and S8) and therefore
590 parameter estimates are less variable. The estimated mutation rate was much lower compared to the main informative prior, with $\mu = 2.474 \cdot 10^{-9}$ [$2.423 \cdot 10^{-9} - 2.612 \cdot 10^{-9}$]. Other parameter
592 estimates are: $\delta = 2.705 \cdot 10^{-3}$ [$2.094 \cdot 10^{-3} - 3.094 \cdot 10^{-3}$], $w_{2n+1} = 1.022$ [$1.021 - 1.024$],
594 $w_{2n+1*} = 1.052$ [$1.05 - 1.054$], $w_{2n^*} = 1.053$ [$1.051 - 1.055$], the latter two being much higher
596 compare to the main informative prior. Notably, the mode of the posterior ratio $w_{2n^*}/w_{2n+1} = 1.0009$ is much lower than the mode of the prior ratio of 1.033 (Figure S3H) and closer to the ratio of 1 that we assume in the main informative prior. Together with the posterior predictive results, we conclude that the main informative prior is preferable over the extended informative prior.

598 **Model with transitions to less-fit genotypes** We also estimated the parameters of a version of the
 model that includes transitions (mutation, chromosome loss and gain) to less-fit genotypes (e.g., $2n^*$
 600 to $2n+1^*$),

$$\begin{aligned} f_{2n}^m &= (1 - \delta - \mu)f_{2n}^s + \delta f_{2n+1}^s + \mu f_{2n+1}^s, \\ f_{2n+1}^m &= \delta f_{2n}^s + (1 - \delta - \mu)f_{2n+1}^s + \mu f_{2n+1}^s, \\ f_{2n+1}^m &= \mu f_{2n+1}^s + (1 - \delta - \mu)f_{2n+1}^s + \delta f_{2n+1}^s, \\ f_{2n}^m &= \mu f_{2n}^s + \delta f_{2n+1}^s + (1 - \delta - \mu)f_{2n+1}^s. \end{aligned} \tag{7}$$

602 The inferred values are slightly different. The estimated mutation rate, $\mu = 1.036 \cdot 10^{-7}$ [$8.01 \cdot 10^{-8} - 1.339 \cdot 10^{-7}$], corresponds to a mutation target size of $\sim 300 - 500$, assuming the mutation
 604 rate per base pair is roughly $2 \cdot 10^{-10}$ (ref.⁶³) or $3.3 \cdot 10^{-10}$ (ref.²⁷). The estimated aneuploidy
 606 rate, $\delta = 2.358 \cdot 10^{-4}$ [$1.766 \cdot 10^{-4} - 2.837 \cdot 10^{-4}$] is 5-35-fold higher than in previous studies:
 608 for chromosome III in diploid *S. cerevisiae*, Zhu et al.⁶³ estimated $6.7 \cdot 10^{-6}$ chromosome gain
 events per generation, and Kumaran et al.²⁶ estimate $3.0 - 4.3 \cdot 10^{-5}$ chromosome loss events per
 610 generation (95% confidence interval). The estimated fitness values are $w_{2n+1} = 1.024$ [1.023 – 1.025],
 612 $w_{2n+1}^* = 1.025$ [1.024 – 1.026], $w_{2n} = 1.032$ [1.031 – 1.033], all relative to the fitness of $2n$, which
 is set to $w_{2n} = 1$. Thus, we can infer that the cost of trisomy is $c = w_{2n} - w_{2n+1}^* = 0.007$ (or 0.7%)
 and the benefit of trisomy is $w_{2n+1} - 1 - c = 0.017$ (1.7%), whereas the benefit of beneficial mutation
 is $w_{2n} - 1 = 0.032$ (3.2%).

We simulated genotype frequency dynamics using parameter samples from the posterior distribution,
 614 and computed the posterior distribution of F_A . The mean F_A in this case is just 0.0189 [0.0004 - 0.1214
 95% CI], lower than without the transitions to less-fit genotypes. Here, F_A is the sum of frequencies
 616 of both $2n_A^*$ and $2n + 1_A^*$, which reaches a frequency of 0.0007. Out of 100,000 posterior samples,
 none had F_A above 0.05 (i.e., 5% of the population).

618 **Supplementary Figures & Tables**

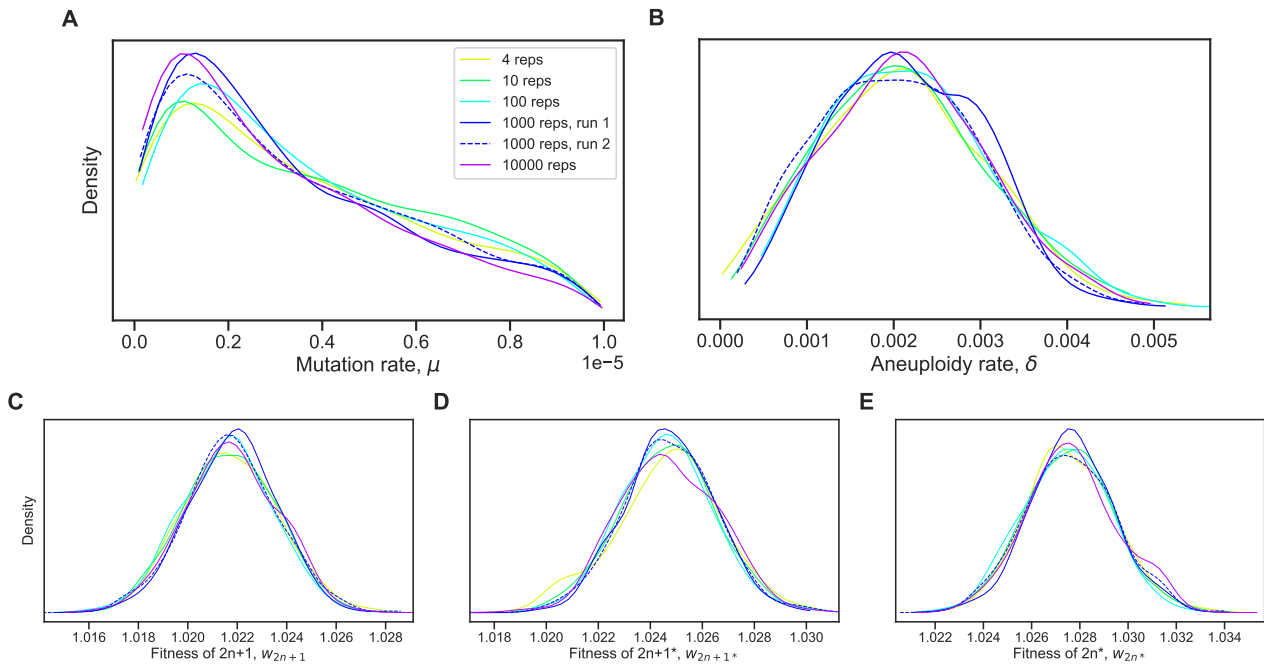


Figure S1: Posterior distribution validation. The posterior distribution of model parameters is roughly the same regardless of the number of simulations (4-10,000 replicates) used to approximate the likelihood (eq. (4)).

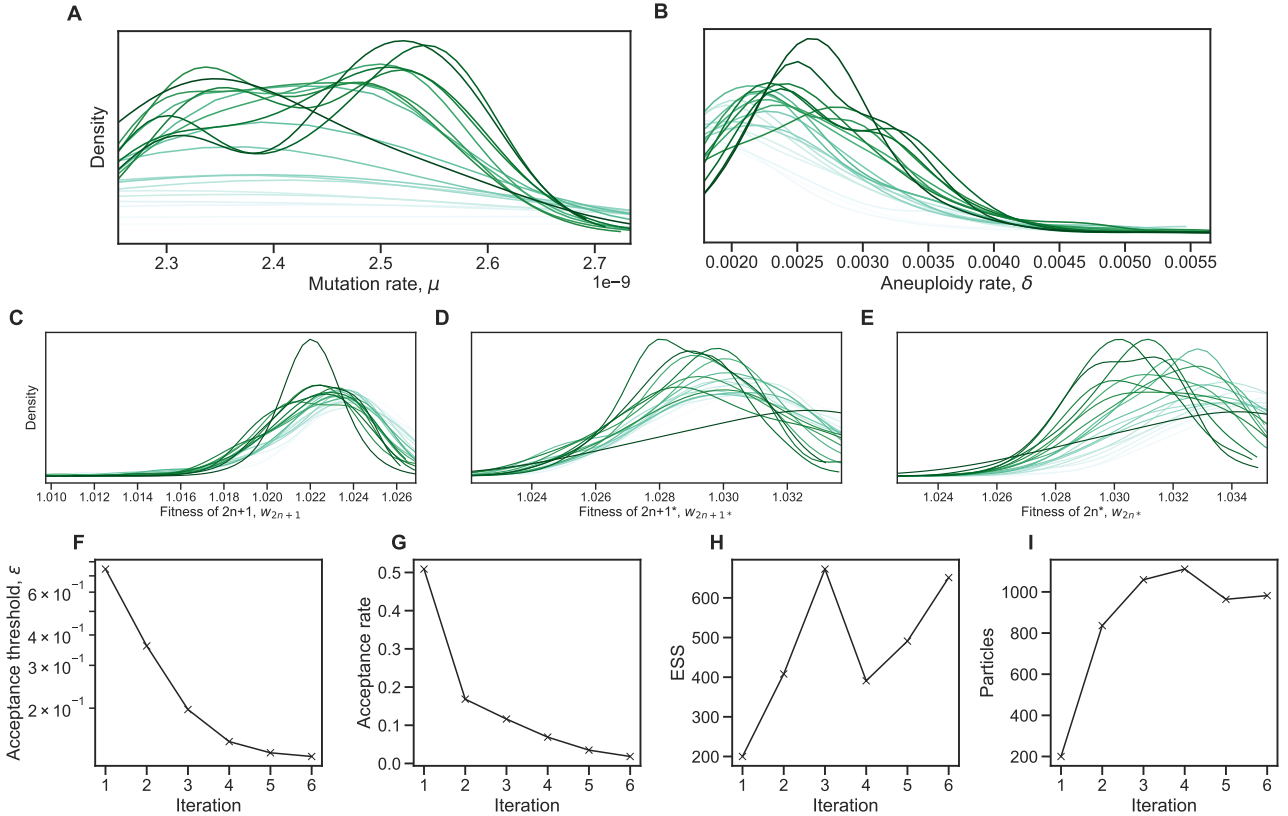


Figure S2: Inference convergence. The ABC-SMC algorithm was used to infer the model parameters. **(A-E)** The approximate posterior distributions of model parameters at each iteration of the ABC-SMC algorithm demonstrates convergence, as the posterior did not significantly change after the first iteration, $t = 1$. **(F-I)** ABC-SMC measures of convergence. After iteration number 6, the acceptance threshold was $\epsilon = 0.13$ (i.e., $\mathcal{L} = 0.87$, eq. (4)), the acceptance rate was 0.018, the number of particles was 982, and the effective sample size ESS=651.

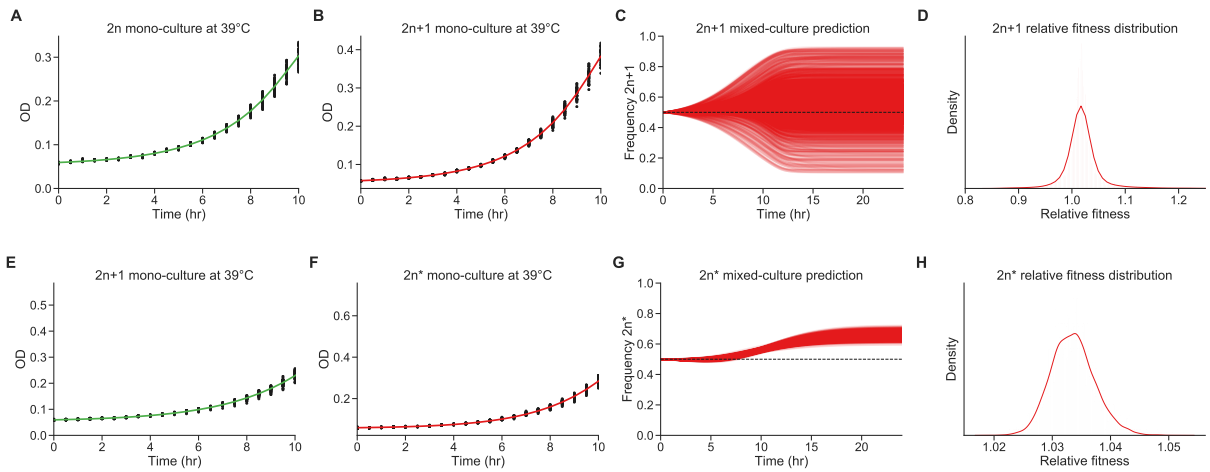


Figure S3: Fitness estimation from growth curves. **(A-D)** Fitness estimation from growth curves of $2n$ and $2n+1$ at 39°C . $w_{2n+1}/w_{2n}=1.024$ (95% CI: 0.959 - 1.115). **Curveball (E-H)** Fitness estimation from growth curves of $2n+1$ and $2n^*$ at 39°C . $w_{2n^*}/w_{2n+1}=1.033$ (95% CI: 1.027 - 1.041). Growth curves previously described in Yona et al.⁵⁹, Figs. 3C, 4A, and S2. Fitness estimated from growth curves using Curveball, a method for predicting results of competition experiments from growth curve data³⁵ curveball.yoavram.com. See *Models and Methods, Prior distributions* for more details. **(A,B;E,F)** Mono-culture growth curve data (markers) and best-fit growth models (lines). **(C,G)** The mixed-culture prediction for the strains from A,B and E,F respectively, 6,375 generated curves. **(D,H)** The relative fitness distribution for $2n+1$ relative to $2n$ (panel D) and $2n^*$ relative to $2n+1$ (panel H). Figures generated by Curveball.

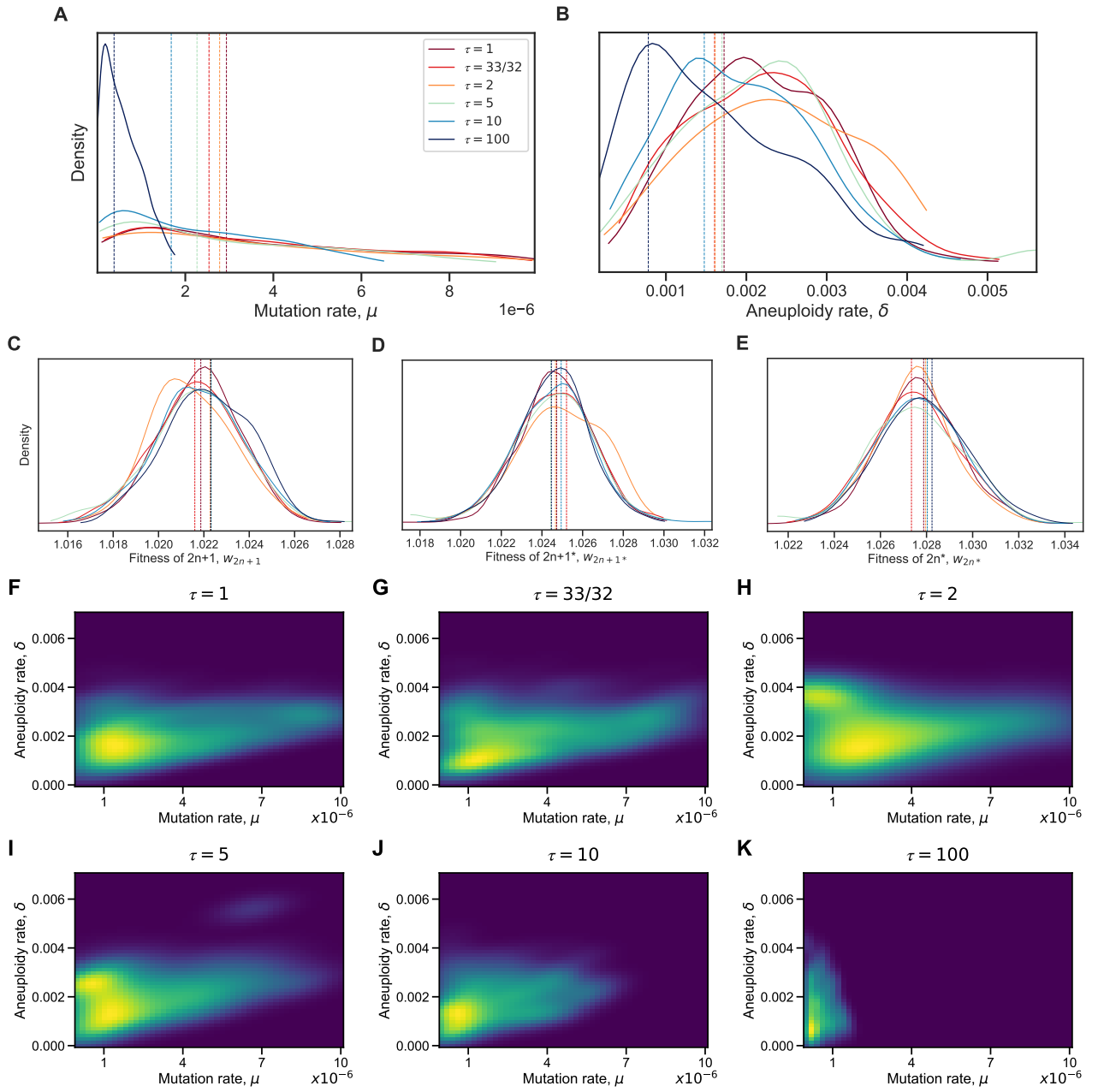


Figure S4: Model with elevated mutation rate in aneuploid cells. (A-E) The inferred posterior distributions for models with different values of τ , the fold-increase in mutation rate in aneuploid cells ($2n+1$ and $2n+1^*$). Vertical dashed lines represent the MAP (maximum a posteriori) of each distribution. When the increase in mutation rate is high, $\tau = 10$ and $\tau = 100$, the inferred mutation (A) and aneuploidy (B) rates tend to be lower. (F-K) The inferred joint posterior distribution of mutation rate (μ) and aneuploidy rate (δ) with different τ values (dark purple and bright yellow for low and high density, respectively).

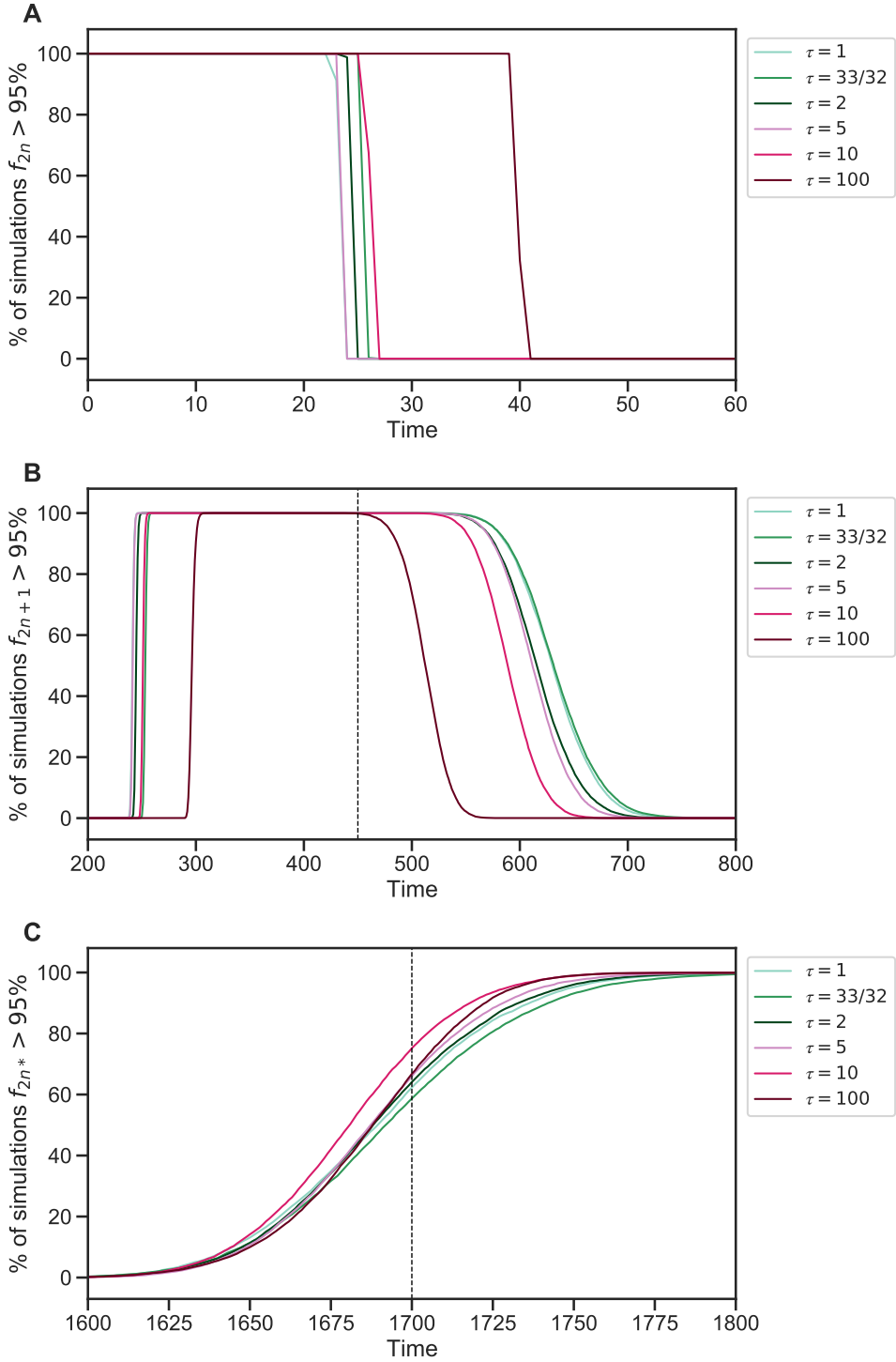


Figure S5: Genotype fixations for models with increased genetic instability. We estimated the parameters for different models, each assuming a different value of τ , the fold-increase in mutation rate in aneuploid cells. We then generated 10,000 simulations using the MAP estimate of each model and evaluated the fraction of simulations in which the frequency of genotype $2n$ (**A**), $2n+1$ (**B**), and $2n^*$ (**C**) is above 95% (y-axis) at each generation (x-axis). Note that $2n+1^*$ did not fix. We can see that $\tau = 100$ can be distinguished if the waiting time for $f_{2n} < 95\%$ is known (panel A) or if the waiting time for $f_{2n+1} > 95\%$ or $f_{2n+1} < 95\%$ is known (panel B). It is harder to distinguish between $1 \leq \tau \leq 10$.

Table S1: Mutant alleles in population $H2$.

Mutant alleles identified in the ancestor (generation 0), aneuploid (generation 450), and evolved (generation 2,350) of population $H2$. See supplementary file.

Table S2: Mutant alleles in population $H4$.

Mutant alleles identified in the ancestor (generation 0), aneuploid (generation 450), and evolved (generation 1,700) of population $H4$. See supplementary file.

Table S3: WAIC values for different τ values.

Model	WAIC
$\tau = 1$	-9
$\tau = 33/32$	-9
$\tau = 2$	-8
$\tau = 5$	-12
$\tau = 10$	-9
$\tau = 100$	-12

WAIC defined in eq. (6).

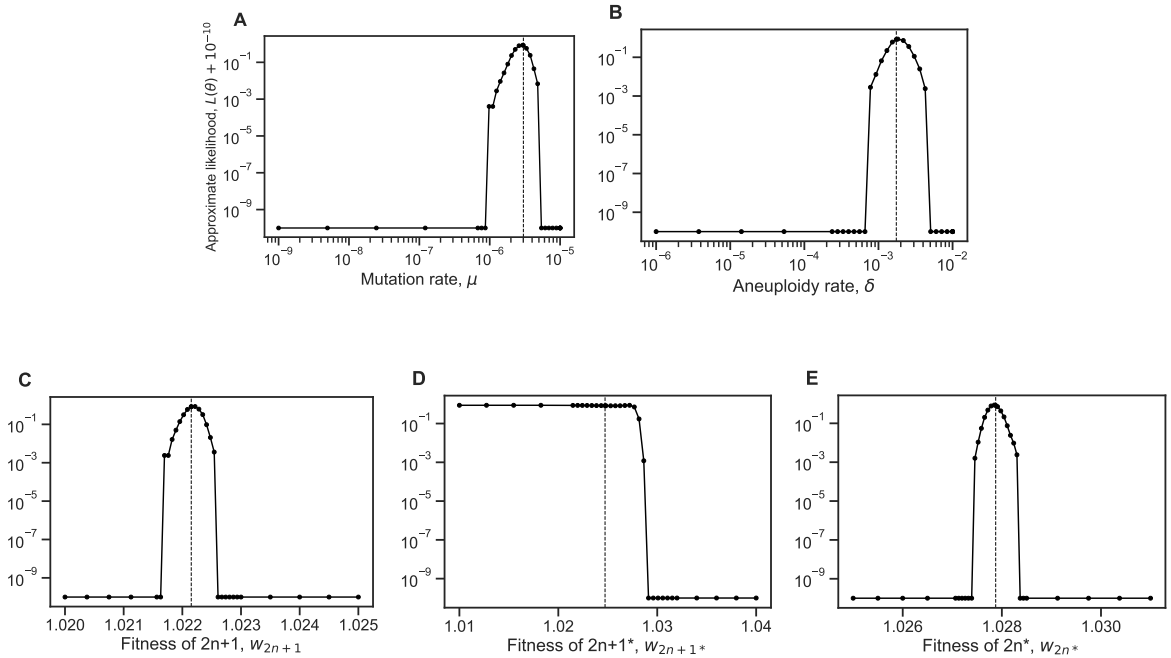


Figure S6: Likelihood profiles. Sensitivity of the model approximate likelihood, $\mathcal{L}(\theta)$, to changing a single parameter while the other parameters remain fixed at their MAP estimates. Dashed vertical line represents the MAP value. The prior distributions for the mutation rate and aneuploidy rate are $\mu \sim U(10^{-9}, 10^{-5})$ and $\delta \sim U(10^{-6}, 10^{-2})$, respectively.

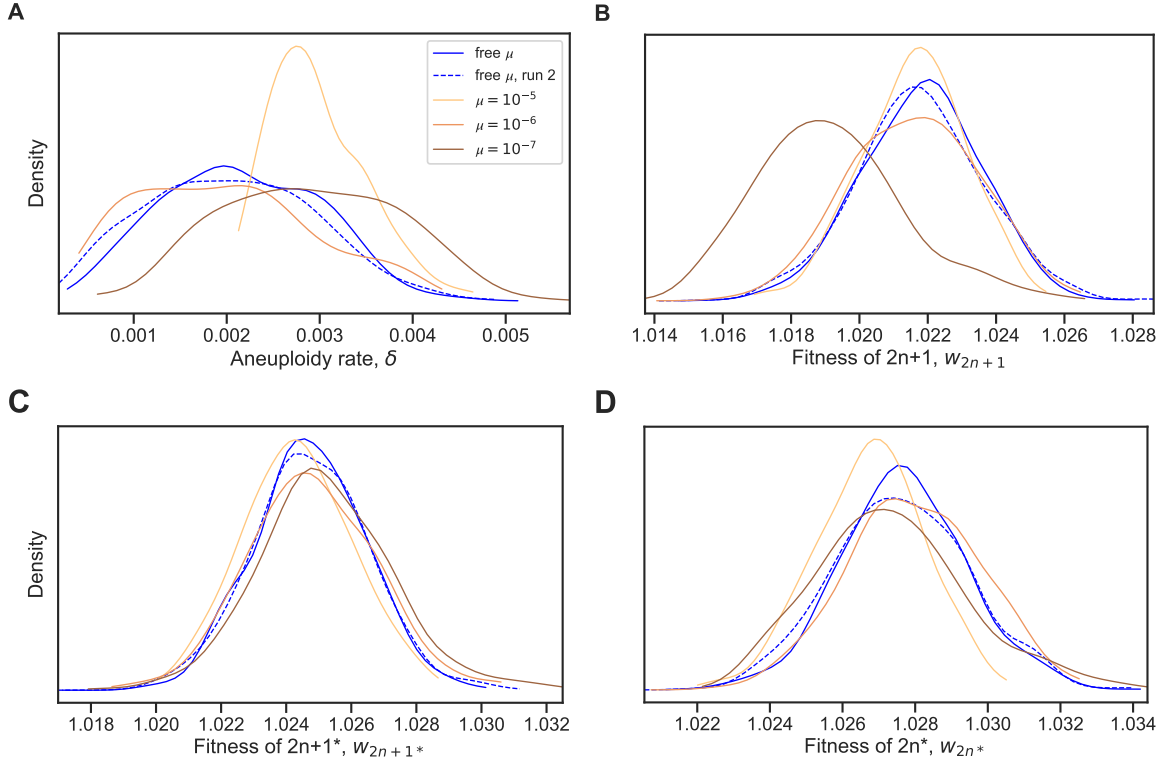


Figure S7: Model with fixed mutation rate. (A-D) The inferred posterior distributions for models with free and fixed mutation rate, μ . The MAP (maximum a posteriori) and 50% HDI (highest density interval) for each model are: **free μ , run 1:** $\delta = 1.720 \cdot 10^{-3}$ [$1.470 \cdot 10^{-3} - 2.786 \cdot 10^{-3}$], $w_{2n+1} = 1.022$ [1.021 – 1.023], $w_{2n+1^*} = 1.025$ [1.024 – 1.026], $w_{2n^*} = 1.028$ [1.026 – 1.029]; **free μ , run 2:** $\delta = 2.129 \cdot 10^{-3}$ [$1.334 \cdot 10^{-3} - 2.695 \cdot 10^{-3}$], $w_{2n+1} = 1.022$ [1.02 – 1.023], $w_{2n+1^*} = 1.025$ [1.023 – 1.026], $w_{2n^*} = 1.028$ [1.026 – 1.029]; **$\mu = 10^{-5}$:** $\delta = 2.903 \cdot 10^{-3}$ [$2.399 \cdot 10^{-3} - 3.156 \cdot 10^{-3}$], $w_{2n+1} = 1.022$ [1.021 – 1.023], $w_{2n+1^*} = 1.024$ [1.023 – 1.025], $w_{2n^*} = 1.027$ [1.026 – 1.028]; **$\mu = 10^{-6}$:** $\delta = 1.917 \cdot 10^{-3}$ [$9.624 \cdot 10^{-4} - 2.447 \cdot 10^{-3}$], $w_{2n+1} = 1.022$ [1.02 – 1.023], $w_{2n+1^*} = 1.025$ [1.023 – 1.026], $w_{2n^*} = 1.028$ [1.027 – 1.029]; **$\mu = 10^{-7}$:** $\delta = 2.901 \cdot 10^{-3}$ [$2.139 \cdot 10^{-3} - 3.671 \cdot 10^{-3}$], $w_{2n+1} = 1.019$ [1.017 – 1.02], $w_{2n+1^*} = 1.025$ [1.024 – 1.026], $w_{2n^*} = 1.027$ [1.026 – 1.029].

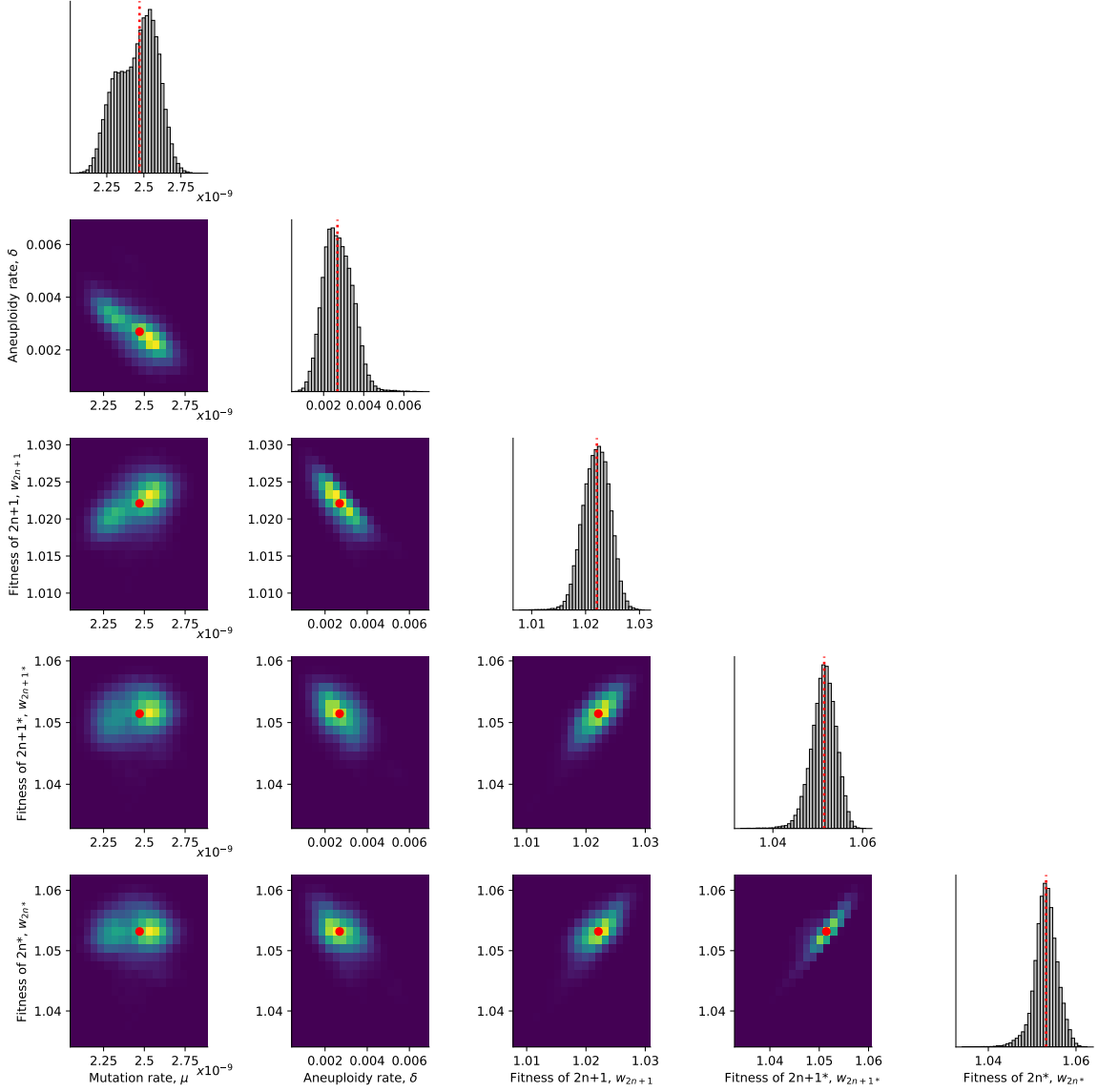


Figure S8: Posterior distribution of parameters inferred with the extended prior distribution. On the diagonal, the inferred posterior distribution of each model parameter. Below the diagonal, the inferred joint posterior distribution of pairs of model parameters (dark purple and bright yellow for low and high density, respectively). Red markers and orange lines for the joint MAP estimate (which may differ from the marginal MAP, as the marginal distribution integrates over all other parameters).

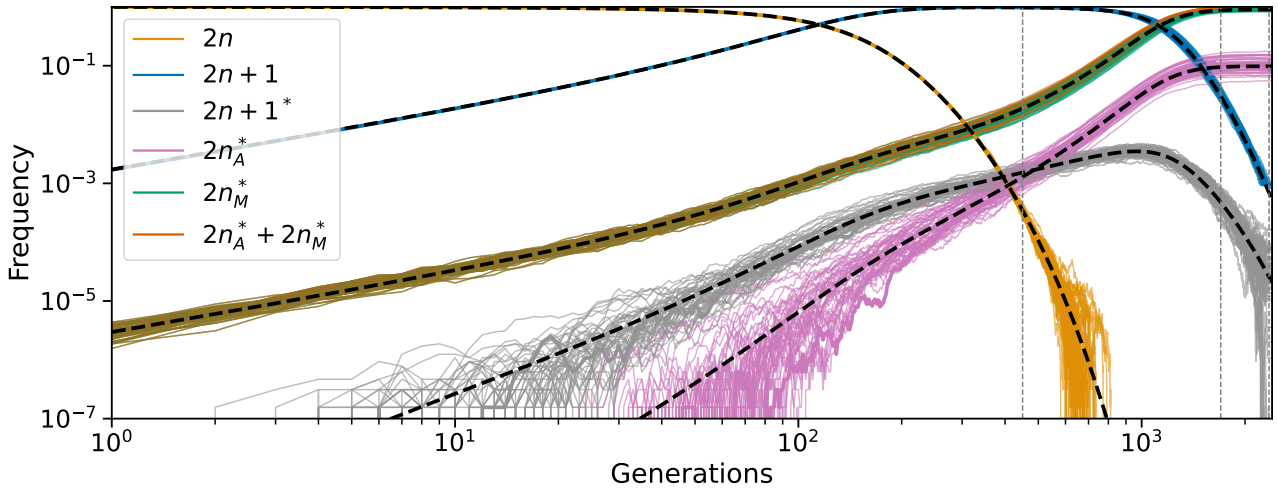


Figure S9: Posterior predicted genotype frequencies in log-log scale. Frequency dynamics of the different genotypes with MAP parameter estimates, same as Figure 5A, but in log-log scale. Black dashed curves for a deterministic model without genetic drift. Clearly, appearance of $2n+1$ and $2n_M^*$ is deterministic. Appearance of $2n+1^*$, and therefore $2n_A^*$, is stochastic, however, the frequency dynamics are deterministic above a frequency of roughly 0.001. Note that the $2n_M^*$ and the $2n_A^* + 2n_M^*$ lines are overlapping for much of their trajectories.

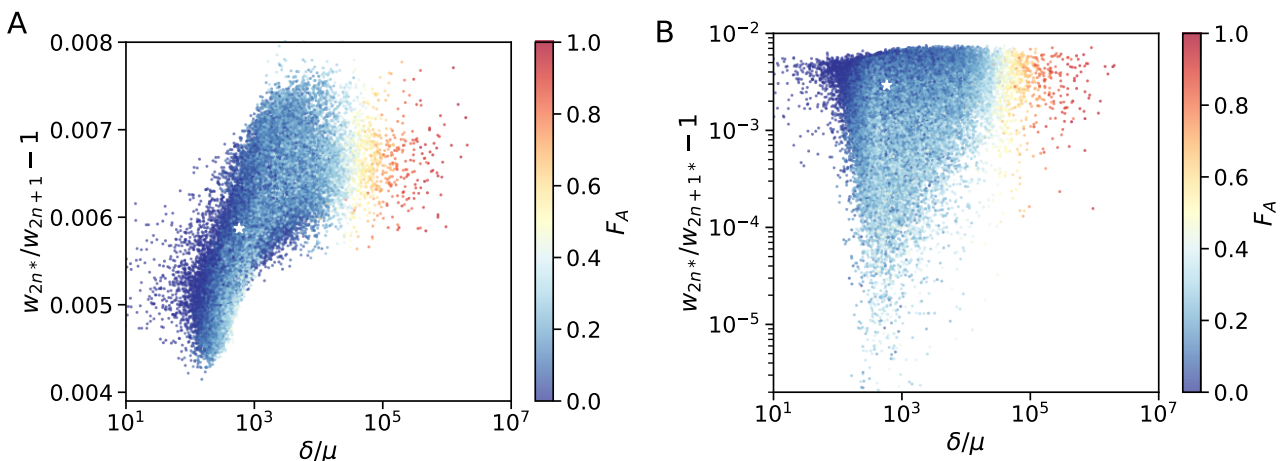


Figure S10: Posterior distribution of F_A . (A,B) F_A values (color coded) as in Figure 5 for different parameter choices on the x- and y-axes. White star denotes the MAP estimate.